

Chapter 1

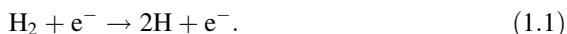
Homoepitaxial Diamond Growth by Plasma-Enhanced Chemical Vapor Deposition

Norio Tokuda

Abstract Both carbon and silicon are group IV members, but carbon has the smaller atomic number. Diamond, with the same crystalline structure as that of silicon, is expected to act as the basic material for the next generation of high-power electronic, optoelectronic, bio/chemical electronic, quantum computing devices, etc. This is because diamond exhibits electrical properties similar to those of silicon, while having superior physical properties. In this chapter, the author reviewed and discussed the homoepitaxial growth of high-quality single-crystal diamond films with atomically flat surfaces, by using plasma-enhanced chemical vapor deposition (PECVD).

1.1 Introduction

Growth of diamond films by chemical vapor deposition (CVD), which has been studied since the 1950s, must be conducted under nonequilibrium conditions. This is because under normal conditions, graphite is a more stable phase of carbon than diamond. Furthermore, during the CVD process, hydrogen radicals (atomic hydrogen) must be present to remove nondiamond carbon, including graphite which is formed on the diamond surface. The hydrogen radicals are generated either by thermal dissociation on a hot filament of W or Ta, or in plasma by electron impact, collisional energy transfer, etc. In plasma, the external energy input couples directly to free electrons, producing hydrogen radicals via



N. Tokuda (✉)

Faculty of Electrical and Computer Engineering, Institute of Science and Engineering,
Kanazawa University, Kanazawa 920-1192, Japan
e-mail: tokuda@ec.t.kanazawa-u.ac.jp

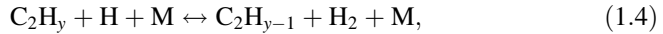
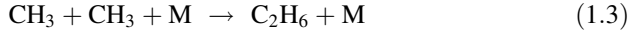
© Springer International Publishing Switzerland 2015

N. Yang (ed.), *Novel Aspects of Diamond*, Topics in Applied Physics 121,
DOI 10.1007/978-3-319-09834-0_1

Methane is commonly used as the carbon source for CVD diamond growth. Activated CH_x ($x = 0, 1, 2, 3$) species are formed by hydrogen abstraction reactions; for example, hydrogen radicals may produce methyl radicals from methane:



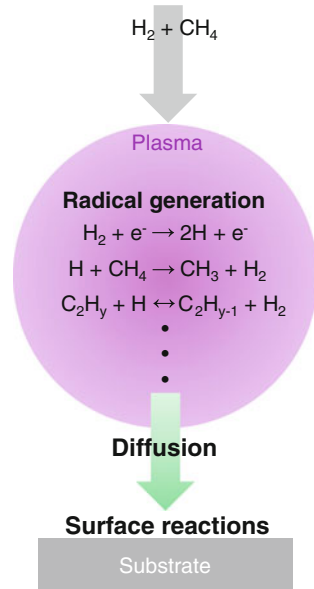
Then, recombination of the methyl radicals induces to form activated C_2H_y ($y = 0, 1, 2, 3, 4, 5, 6$) species:



where M is a third body. The CH_x and C_2H_y radicals are regarded as precursors for diamond growth during the CVD process, as shown in Fig. 1.1 [1–8]. Thus, radicals play an important role in CVD diamond growth; this differs from the other semiconductor films' growth conducted by nonplasma processes such as thermal CVD and molecular beam epitaxy.

Hot-filament CVD has been applied to large-scale industrial processes because of its simple system configuration and ability to coat large areas and complex shapes. However, hot-filament CVD of diamond films must be carried out at lower gas temperatures and pressures than those of plasma CVD because of the upper temperature limit of the filament materials and the low production rate of hydrogen radicals. This leads to relatively low growth rates of diamond films compared to

Fig. 1.1 Schematic of CVD diamond processes



diamond growth by plasma-enhanced CVD (PECVD). Recently, homoepitaxial diamond growth rates of $>100 \mu\text{m/h}$ by PECVD have been reported [9–15]. Additionally, both *p*- and *n*-type diamond films have been reproducibly grown by PECVD [16–42]. Therefore, the diamond films used in diamond electronic devices were grown by PECVD [43–75].

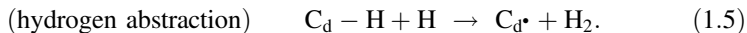
In this chapter, recent studies on homoepitaxial diamond growth by PECVD are reviewed. Additionally, impurity doping into diamond and the growth of atomically flat diamond surfaces are described.

1.2 Growth Mechanism

More than a decade has passed since PECVD of diamonds was established. Since then, many experimental and theoretical studies have been reported. Diamond growth by PECVD is not driven by thermodynamics but by the chemistry and kinetics of vapor phase and surface reactions. To elucidate the diamond growth mechanism during PECVD, both vapor-phase and surface reactions need to be understood. Evaluations of the vapor phase have been based on optical emission spectroscopy (OES) and mass spectrometry (MS) [76–83]. Here, as described in Sect. 1.1, the production and diffusion of hydrogen, CH_x radicals, and C_2H_y radicals are key processes, as shown in Fig. 1.1. Recently, the distributions of the radical, gas, and electron temperatures in plasmas have been simulated [84–94]. The simulation results provide some information on vapor-phase reactions in the CVD diamond process, but microscopic experimental results are still needed. Those radicals that arrive at diamond surfaces migrate and react with hydrogen, terminating the surface and/or carbon. It is extremely challenging to identify the involved processes because of the difficulty of conducting in situ characterizations in plasma environments. In this section, the author reviewed only those aspects of diamond surface chemistry that pertain to chemical reactions of hydrogen radicals and diamond precursors (CH_x and C_2H_y radicals).

1.2.1 Hydrogen

During diamond growth by PECVD, the diamond surfaces are continuously bombarded with hydrogen radicals. While under typical growth conditions, the hydrogen concentration is 95 % or higher (the hydrogen concentration is defined as the ratio of hydrogen flow rate to total gas flow rate). Consequently, most diamond surfaces are terminated by hydrogen and cannot react with diamond precursors. However, hydrogen radicals abstract the hydrogen from terminated diamond surfaces, $\text{C}_d\text{-H}$, to form an active site, $\text{C}_d\bullet$:



Then, the active site contributes to the diamond growth, but there is also a large possibility that, the active site again reacts with a hydrogen radical and is terminated again with hydrogen.

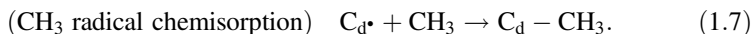


During diamond growth by PECVD, the fraction of active sites is determined by the dynamic equilibrium between chemical reactions (1.5) and (1.6). The diamond surfaces after the hydrogen plasma treatment and diamond growth by PECVD are terminated by hydrogen, as shown in Fig. 1.2.

Hydrogen radicals also play a role in the growth of high-quality diamond films by removing nondiamond carbon. Diamond is etched by reactions with hydrogen radicals, although the etching rate is lower than that of nondiamond carbon. The diamond etching rates by hydrogen radicals depend on the structures on the diamond surface: monohydride (CH), dihydride (CH₂), and trihydride (CH₃). Chen et al. proposed that the diamond etching rates, R , by hydrogen radicals are $R_{\text{monohydride}} < R_{\text{dihydride}} < R_{\text{trihydride}}$ [95]. They also reported that {111}-oriented facets form on both single-crystal diamond {110} and {100} surfaces by anisotropic etching. Thus, diamond growth by PECVD is accompanied by the reactions of hydrogen abstraction (1.5) and adsorption (1.6) and by anisotropic etching on diamond surfaces, which limits chemisorption of diamond precursors and diamond nucleation.

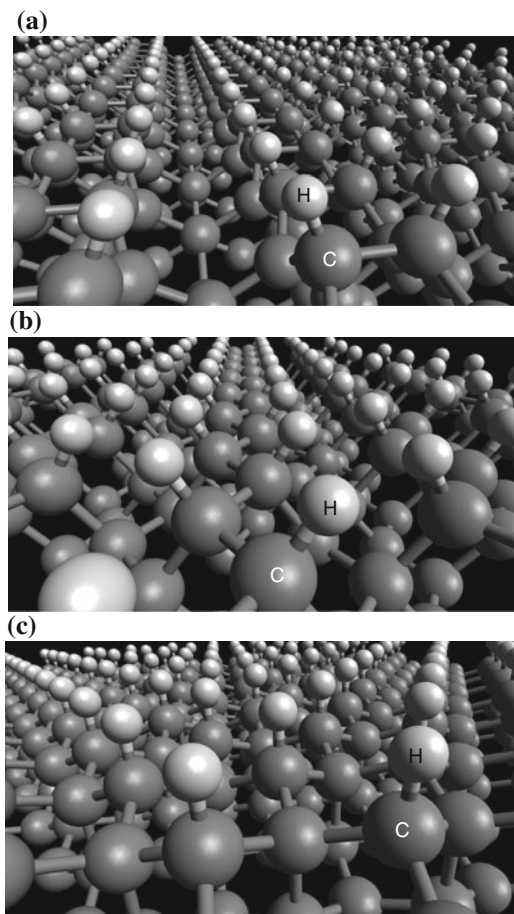
1.2.2 Carbon

As described in Sect. 1.2.1, diamond surfaces are nearly fully terminated by hydrogen during diamond growth by PECVD. Chemisorption by diamond precursors occurs not at hydrogen-terminated sites but at active sites, which are hydrogen-abstracted sites:



The chemisorbed structure is a trihydride, which is readily etched by hydrogen radicals. Structures composed of monohydrides and/or dihydrides may need to nucleate on diamond surfaces during PECVD. Observation of the growth surface is crucial for elucidation of the growth mechanism because the growth process influences the structure of the growth surface. Scanning probe microscopy (SPM), low-energy electron diffraction (LEED), Fourier transform-infrared spectroscopy (FT-IR), and electron energy loss spectroscopy (EELS) provides physical and chemical information on surfaces at the atomic level, and are powerful tools for the study of diamond CVD growth. Results from such techniques reveal that as-grown diamond {100} and {111} surfaces have 2×1 :H reconstructed structures with

Fig. 1.2 Hydrogen-terminated diamond {100}, {110}, and {111} surfaces.
a H-terminated diamond {100} surface.
b H-terminated diamond {110} surface. **c** H-terminated diamond {111} surface



carbon dimer rows and 1×1 :H structures, respectively [96–108]. Nevertheless, at present, the mechanism of diamond growth by PECVD is still not well-understood because of the difficulty of in situ observations.

1.3 Growth Modes

To realize diamond-based electronics, a growth technique is needed for producing device-grade diamond films. As described in Sect. 1.2, the growth mechanism of diamond films by PECVD remains poorly understood because of the difficulty of in situ characterization in plasma environments [109]. Additionally, the control of dynamic characterizations on well-defined surfaces, such as a scanning electron

or probe microscope-molecular beam epitaxy system used for Si [110], GaAs [111], and GaN [112], is needed to elucidate the growth mode of PECVD diamond films.

Figure 1.3 illustrates a simplified model for the determination of growth modes by an alternative to in situ characterizations [113, 114]. Figure 1.3 illustrates the surface steps present on an ideal surface of an as-received diamond substrate after the formation of a mesa structure due to a misoriented angle between the basal plane and polished surface. Then, homoepitaxial growth is carried out under a lateral growth mode without 2D nucleation on terraces, as described below. Each atomic step on the mesa surface grows laterally. Under ideal conditions in which 2D terrace nucleation is completely suppressed, there would be no further growth perpendicular to the basal plane. Finally, a step-free surface is formed over the mesa surface, leaving the basal plane surface. In 2D island growth, new steps are formed by nucleation on the terraces during lateral growth. Finally, a surface with single atomic steps and atomically flat terraces is formed on the mesa surface. The interval between the formed islands is wider than the terrace width estimated from the misoriented angle of the substrate. In 3D growth, the interval between the formed islands is narrower than the terrace width estimated from the misoriented angle. As a result, the surface is very rough. In addition, this mesa structure eliminates the influence of abnormal growth, such as spiral growth induced by screw dislocations from trench bottoms. Thus, diamond growth modes can be determined from ex situ surface observations of diamond films grown on mesa surfaces.

Figure 1.4 shows atomic force microscopy (AFM) images of diamond {111} mesa surfaces before and after homoepitaxial growth by PECVD. For diamond growth at low methane concentrations (0.005–0.025 % $\text{CH}_4/(\text{H}_2+\text{CH}_4)$ ratio), a step-free surface, that is, a perfectly flat surface without any atomic steps, was formed on the mesa. This result shows that the growth mode of the homoepitaxial diamond {111} films was an ideal lateral growth without 2D terrace nucleation. For diamond growth at middle methane concentrations (0.05–0.25 % $\text{CH}_4/(\text{H}_2+\text{CH}_4)$ ratio), equilateral-triangular islands and/or single bi-atomic layer step/terrace structures on atomically flat surfaces were formed on the mesa. This shows that the growth mode of the homoepitaxial diamond {111} films is 2D island growth with 2D terrace nucleation and lateral growth. Additionally, the formation of equilateral-triangular islands shows that the diamond growth had extremely high selectivity. For diamond growth at high methane concentrations (>0.25 % $\text{CH}_4/(\text{H}_2+\text{CH}_4)$ ratio), the film surface, whose RMS value was 0.84 nm, is much rougher than the initial surface before growth (RMS = 0.44 nm). This shows that the growth mode for the homoepitaxial diamond {111} films is 3D growth.

Variations in methane concentrations give rise to different fluxes of hydrocarbon precursors arriving at the surface. This is because growth rates increase with methane concentration. Since the substrates used for growth have the same misoriented angle, the concentrations of adatoms on terraces increase with higher methane concentrations. When the flux is low, adatoms on a terrace remain below the critical size for 2D terrace nucleation. Adatoms, which are adsorbed precursors on the diamond surface, arriving at steps crystallize, resulting in step-edge growth (no 2D terrace nucleation).

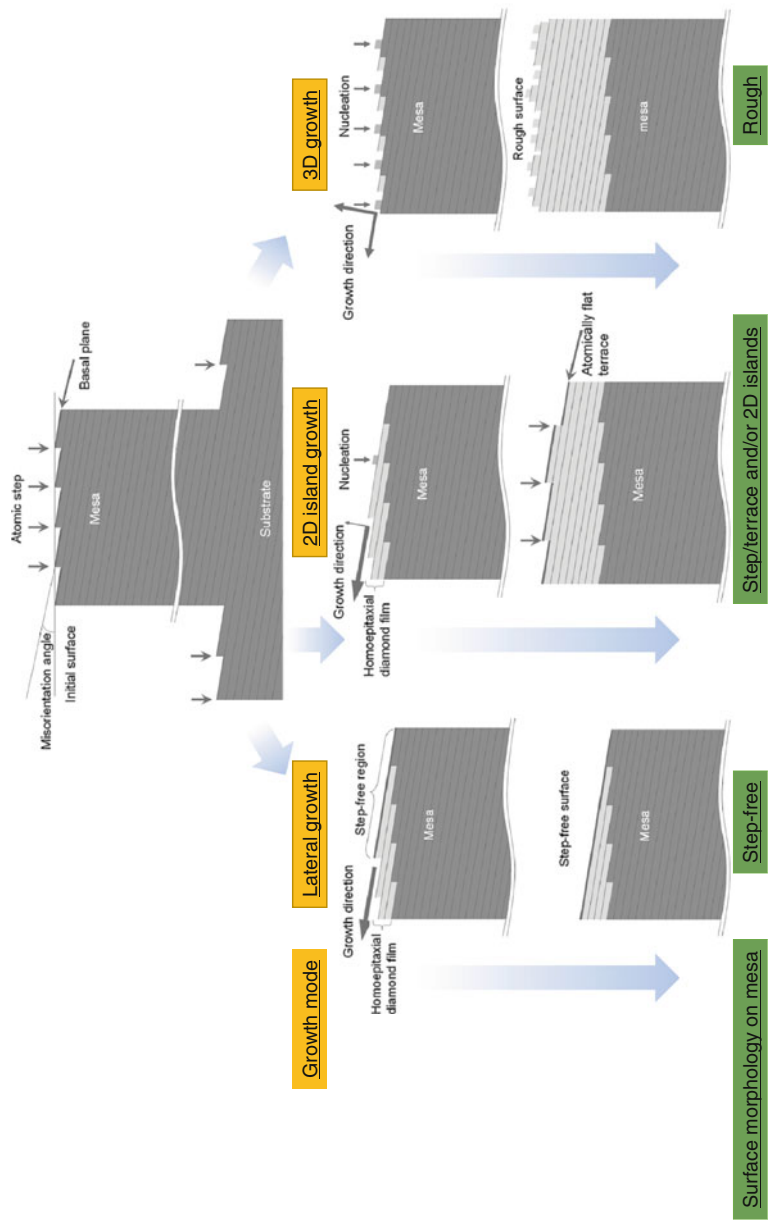


Fig. 1.3 Simplified models for the determination of growth modes by using mesa structures

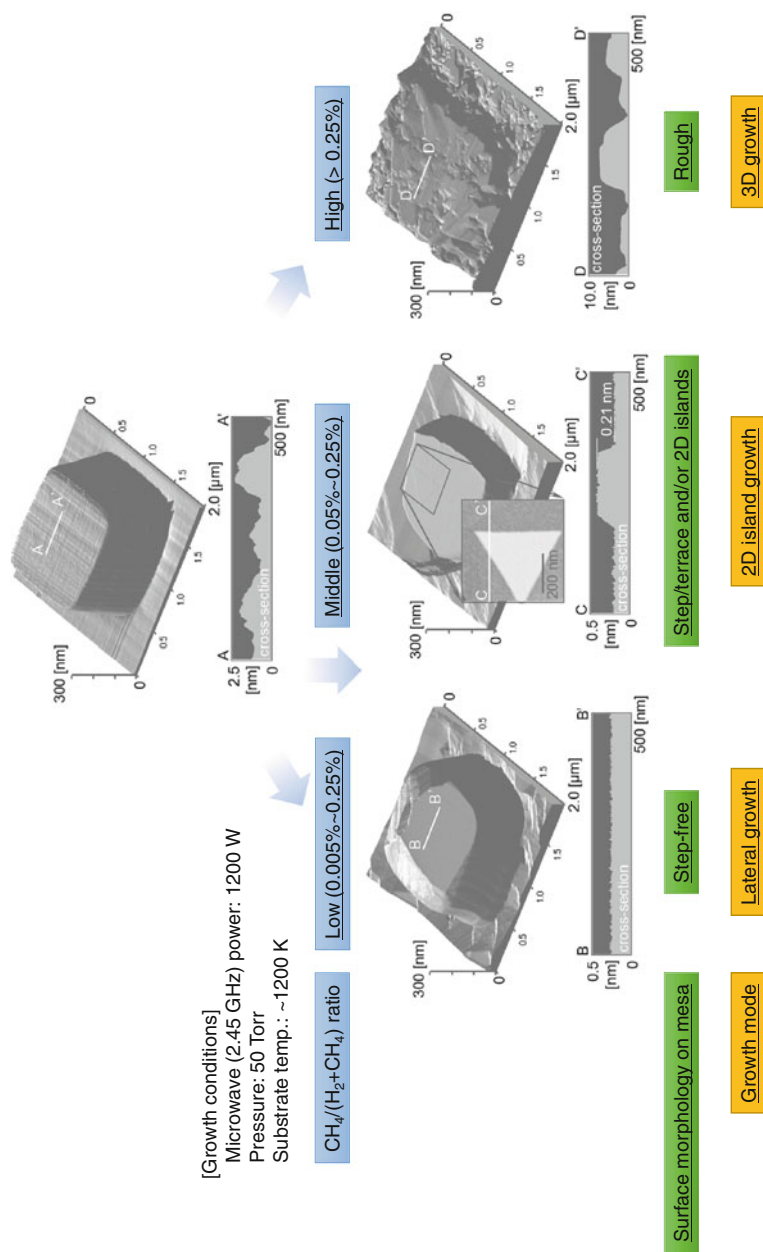


Fig. 1.4 AFM images of diamond {111} mesa surfaces before and after homoepitaxial growth by PECVD

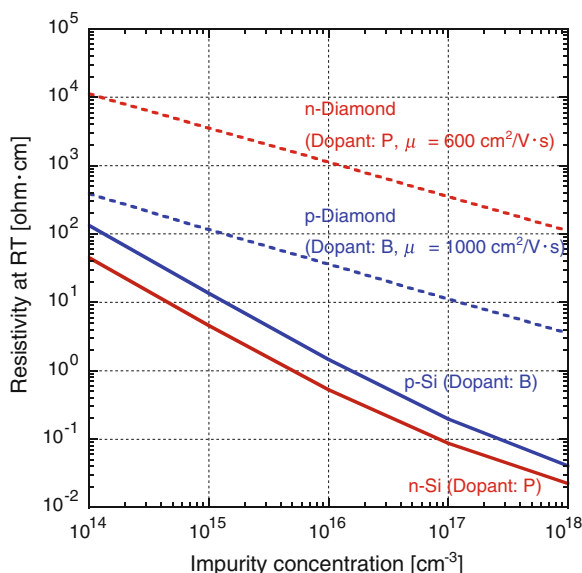
In the middle methane concentration region, the adatom concentration increases and passes the critical value needed for 2D nucleation. Adatoms can cluster more easily on terraces because of their higher population. This causes 2D nucleation on terraces. As the methane concentration is increased further (into the high methane concentration region), adatoms form clusters as soon as they land on surfaces from the gas phase. This causes surface roughening because of 3D growth. This growth mechanism is a common process in thermal CVD and MBE. Despite the extremely short migration length, the common mechanism may also apply to PECVD diamond {111} growth because of the formation of atomically flat surfaces of diamond films.

1.4 Doping

For the realization of diamond-based electronic devices, doping acceptor and donor impurities into diamond is necessary to control the carrier type and concentration and to control the electrical resistivity of diamond semiconductors. Nitrogen is the most common impurity in diamond. Nitrogen is likely to form several types of complexes with vacancies. Recently, the nitrogen-vacancy (N–V) center in diamond has attracted much attention as a promising solid-state spin system for quantum information and sensing applications [71, 115–123]. However, as a donor, nitrogen in diamond has a high activation energy of 1.7 eV, which is higher than the bandgap of silicon (1.1 eV). The resistivity of nitrogen-doped diamond is extremely high at room temperature because of the extremely low concentration of thermally activated electrons. Generally, boron and phosphorus are used as *p*- and *n*-type dopants of diamond semiconductors, respectively. The activation energies of boron- and phosphorus-doped diamond are 0.37 and 0.57 eV, respectively, which are lower than that of nitrogen-doped diamond. However, compared with boron- and phosphorus-doped silicon, the resistivity of doped diamond is still too high, as shown in Fig. 1.5. Although other dopants with lower activation energies have been investigated, reproducibility has not yet been obtained.

Doping into diamond is carried out by HPHT, PECVD, and ion implantation [124–129]. Recently, Bormashov et al. reported that boron-doped {100} diamond without any extended defect. It was synthesized by HPHT and showed the high Hall hole mobility of 2,200 cm²/V s at 300 K and 7,200 cm²/V s at 180 K [130]. For device fabrication, doped diamond films are mostly grown on HPHT or CVD diamond substrates by PECVD because doping by PECVD provides both *p*- and *n*-type diamond with controlling concentrations of impurities. During homoepitaxial diamond growth by PECVD boron and phosphorus doping is carried out by introducing diborane (or trimethylboron) and phosphine (or tertiarybutylphosphine) gases, respectively. The highest Hall hole and electron mobility of PECVD diamond films are 1,860 cm²/V s at 290 K [131] and 660 cm²/V s at 300 K [34], respectively. Carrier mobility decreases with increasing boron or phosphorus concentrations in diamond films, reducing the resistivity of diamond. For [B] < 10¹⁹ cm⁻³, conduction

Fig. 1.5 Room-temperature resistivities of Si and diamond as functions of impurity concentration. The resistivities of *p*- and *n*-type diamond were calculated when the compensation ratio was zero and mobility was constant



is dominated by free holes in the valence band. At higher doping concentrations, variable-range hopping conduction appears, and then the metal-insulator transition and superconductivity arise around 3×10^{20} B atoms/cm³ [132–138]. The resistivity of heavily boron-doped diamond {100} film with 3×10^{20} B atoms/cm³ is 10 mΩ cm or less at room temperature [132, 139–141]. In contrast, the resistivity of heavily phosphorus-doped diamond {111} film with 10^{20} P atoms/cm³ is around 70 Ω cm at room temperature [142]. These can lead to the fabrication of chemical/bio and electronic devices, such as Schottky barrier diodes, *pn*-junction diodes, Schottky *pn* diodes, JFETs, and bipolar transistors.

1.5 Growth of Atomically Flat Diamond

To realize electronic devices with proper performance characteristics, one of the most important issues is the roughness of surfaces and interfaces in semiconductor materials. Device applications of diamond semiconductors require sharp interfaces at diamond homo- and hetero-junctions. Generally, growth of *p*- and *n*-type diamond semiconductors for Schottky contacts and *pn* junctions, etc., is carried out by boron and phosphorus doping, respectively, during homoepitaxial diamond growth. However, growth hillocks, which are macroscopic defects, are often observed on as-grown diamond surfaces after homoepitaxial diamond growth by PECVD, as shown in Fig. 1.6. In most cases, even macroscopic flat surfaces excluding hillocks are not atomically flat, as shown in Fig. 1.7. Therefore, surface flattening of homoepitaxial diamond films is extremely important.

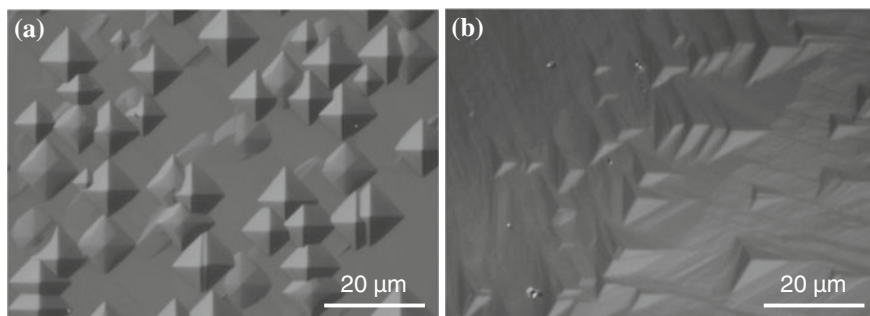


Fig. 1.6 OM images of hillocks formed on diamond surfaces after homoepitaxial growth by PECVD. **a** Quadrangular hillocks were observed on diamond {100} surfaces and **b** triangular hillocks on diamond {111} surfaces

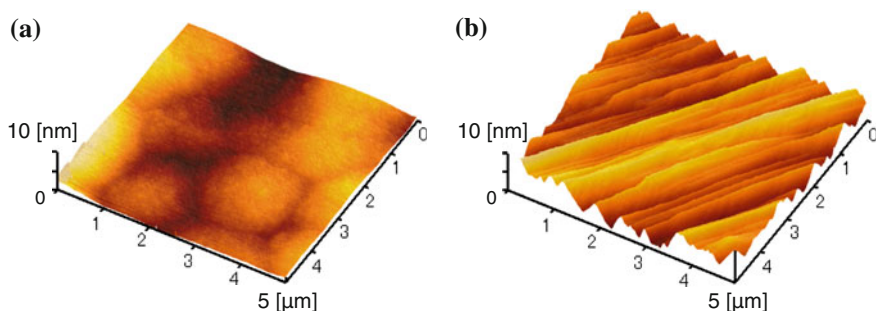


Fig. 1.7 3D AFM images of diamond surfaces, excluding hillocks, after homoepitaxial growth by PECVD. **a** The surface roughness (RMS) of the homoepitaxial diamond {100} film was 0.54 nm. **b** The surface roughness (RMS) of the homoepitaxial diamond {111} film was 1.68 nm

Surface flattening can be carried out by a polishing process. For example, defect-free Si wafers with surface flatness at the atomic level can be obtained by chemical–mechanical polishing. However, as-received diamond substrate surfaces are not atomically flat; instead, they have a roughness of several nanometers or more after mechanical polishing, as shown in Fig. 1.8. Compared with as-received Si wafer surfaces after chemical–mechanical polishing, as shown in Fig. 1.9, diamond surfaces are much rougher. Recently, a new technique for diamond surface polishing has been reported [143–145]. It is expected that surface roughness of diamond substrates will be reduced to that of Si wafers via some breakthrough diamond polishing technique. In this section, the author describe the growth of hillock-free, atomically step/terrace, and step-free diamond films.

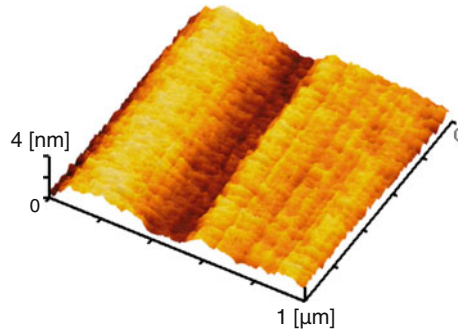


Fig. 1.8 3D AFM image of as-polished single-crystal diamond surface after acid treatment. The surface roughness (RMS) was 0.44 nm

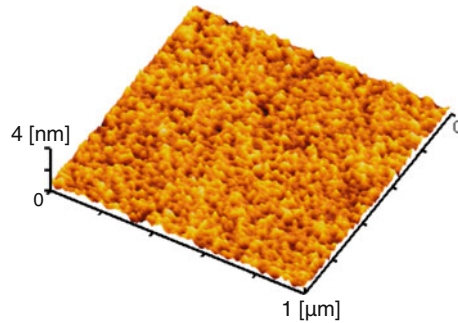


Fig. 1.9 3D AFM image of as-polished single-crystal Si surface after modified RCA cleaning. The surface roughness (RMS) was 0.16 nm

1.5.1 Hillock-Free Surfaces

Growth hillocks are often observed on homoepitaxial diamond {100} and {111} surfaces, as shown in Fig. 1.6. A growth hillock is formed by spiral growth centered on a screw dislocation core, as shown in Fig. 1.10 [114, 146], and the diamond surface is increasingly roughened by the growth of hillocks. The spiral growth rate at a screw dislocation is higher than the normal growth rate on the surface, excluding such crystal defects. Generally, growth hillocks make device fabrication difficult; hillocks are related to dielectric breakdown and current leakage in electronic devices such as *pn* junctions, Schottky contacts, and MIS structures. Therefore, it is extremely important to eliminate hillocks from epitaxial diamond films. The most effective method for achieving hillock-free diamond is to completely eliminate dislocations from single-crystal diamond. However, dislocation-free diamond substrates are very expensive compared to common single-crystal diamond substrates with dislocation densities of 10^4 – 10^5 cm⁻². Alternatively, it is

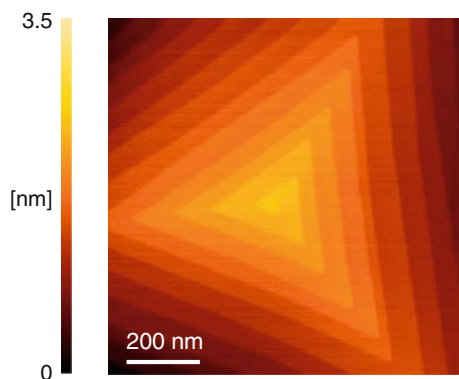


Fig. 1.10 AFM image of spirally grown diamond $\{111\}$ film due to screw dislocation. Each step height was approximately 0.21 nm, which is consistent with the single BL step height of $\{111\}$ diamond

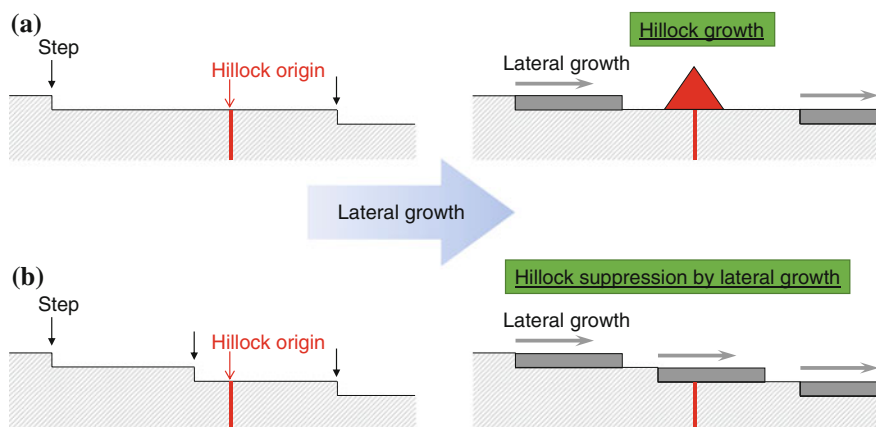


Fig. 1.11 Simplified models of hillock growth and suppression on samples having (a) low and (b) high misorientation angles θ by lateral growth

possible to eliminate hillocks by homoepitaxial lateral growth on highly misoriented diamond substrates. Figure 1.11 shows a simple model for suppressing the growth of hillocks [141]. The mechanism of hillock formation during diamond growth is considered to be as follows. The origins of hillocks have a growth rate higher than those of other areas. A local increase in growth rate due to the defects observed by transmission electron microscopy, which are dislocations [147] and twinning structures [148], has been reported. Hence, growth at the origins of hillocks could be suppressed when the growth rate of a normal epitaxial area exceeds that of hillocks, indicating an enhancement of lateral growth.

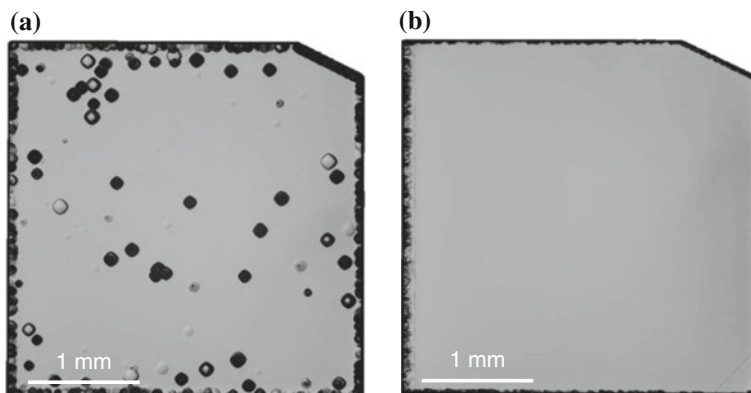


Fig. 1.12 OM images of homoepitaxial diamond film surfaces on single-crystal diamond {100} substrates with (a) low and (b) high misorientation angles, θ . The low and high values of θ were 0.2 and 2.2, respectively. The homoepitaxial diamond films were grown under the same conditions (1,200 W, 50 Torr, 0.6 % $\text{CH}_4/(\text{H}_2+\text{CH}_4)$ ratio, 1.6 % B/C ratio, 70 h) [141]

Figure 1.12 shows the optical microscopy (OM) images of homoepitaxial diamond films grown on diamond {001} substrates with (a) $\theta = 0.2^\circ$ and (b) $\theta = 2.2^\circ$. Hillocks were observed to spread over the entire surface of the low- θ sample, as shown in Fig. 1.12a. The density and size of the hillocks were $2 \times 10^3 \text{ cm}^{-2}$ and below 200 μm , respectively. The Hillock size increases with film thickness, and thus, the film surface becomes rough macroscopically. This roughening is a fatal issue for the additional growth of homoepitaxial diamond films intended for device fabrication. However, suppression of hillock growth can be achieved by increasing θ to above 2° [141]. The OM image of the high- θ sample is shown in Fig. 1.12b. Judging from this image, a hillock-free diamond film with a macroscopically flat surface was obtained over the entire surface by homoepitaxial lateral growth on highly misoriented substrates.

1.5.2 Step/Terrace Structures

As described in Sect. 1.5.1, it is possible to obtain a hillock-free diamond film with a macroscopically flat surface by homoepitaxial lateral growth on a highly misoriented substrate. In most cases, the homoepitaxial lateral growth of diamond films accompanies 2D terrace nucleation. Therefore, macroscopically flat diamond surfaces, excluding hillocks, after homoepitaxial growth are not atomically flat but roughened because of 2D terrace nucleation, as shown in Fig. 1.7. Therefore, it is necessary to suppress 2D terrace nucleation during homoepitaxial growth by PECVD.

Fig. 1.13 AFM image of atomically flat diamond {100} surfaces after homoepitaxial lateral growth at a low methane concentration (0.05 %)

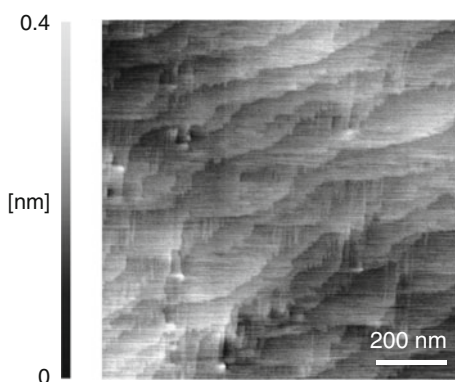
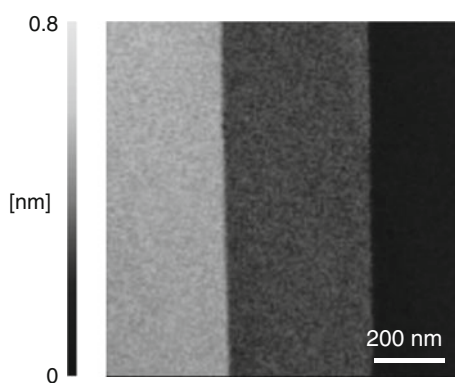


Fig. 1.14 AFM image of atomically flat diamond {111} surfaces after homoepitaxial lateral growth at a low methane concentration (0.05 %)



Watanabe et al. successfully formed an atomically flat diamond {100} film over the entire substrate by homoepitaxial lateral growth at extremely low CH_4/H_2 ratios [149]. Figure 1.13 shows an AFM image of an atomically flat diamond {100} surface by such a growth. The step heights were approximately 0.1 nm, which is consistent with the single atomic step of {100} diamond (0.089 nm), or 0.2 nm, which is consistent with the bi-atomic step of {100} diamond (2×0.089 nm). The average interval between steps (66 nm) is consistent with the estimated terrace width from the misorientation angle of the diamond {100} substrate (65 nm).

Atomically flat diamond {111} surfaces were also formed by homoepitaxial lateral growth, as shown in Fig. 1.14. The step height was approximately 0.2 nm, which is consistent with the single atomic step of {111} diamond (0.206 nm). The atomically flat diamond {111} surfaces with step/terrace structures were selectively formed by lateral growth on a diamond {111} substrate with mesa structures [150, 151].

1.5.3 Atomically Step-Free Surfaces

Much effort has been expended on flattening the surfaces of Si, GaAs, SiC, and GaN at the atomic level; those efforts have led to the achievement of perfectly flat surfaces without any atomic steps (atomically *step-free* surfaces) through step-flow growth without 2D nucleation on terraces [152–156]. The aluminum nitride (AlN)/diamond heterostructure is expected to combine the features of both wide-bandgap materials, thereby providing a new scheme for both nitride and diamond devices because they have opposite tendencies in doping characteristics [157–161]. Hirama et al. reported that single-crystal AlN {0001} growth on a diamond {111} surface was achieved [160], but the AlN layer on a diamond {100} surface had a multidomain structure consisting of tilted and rotated domains [162]. To realize useful devices, high-quality AlN films on {111} diamond and sharp AlN/diamond {111} interfaces are essential. For GaN/SiC heterostructures, previous studies have revealed that surface steps promote extended crystal defects in heteroepitaxial films grown on SiC [163–165]. Bassim et al. reported that very low dislocation densities were achieved in GaN films on step-free SiC mesa surfaces [166], and ultraviolet luminescence of GaN *pn*-junction diodes fabricated on the step-free SiC {0001} surfaces was improved relative to that on atomically flat SiC surfaces with atomic steps [167]. Thus, the formation of step-free diamond surfaces is a promising technique for improving the performance of devices that use diamond heterostructures.

Two methods for the formation of *step-free* surfaces have been proposed, as shown in Fig. 1.15. Both methods utilize an ideal lateral growth mode without 2D terrace nucleation. In method I, a mask, which is not etched and on which no nucleation occurs in the growth environment, is used for selective growth. Method II,

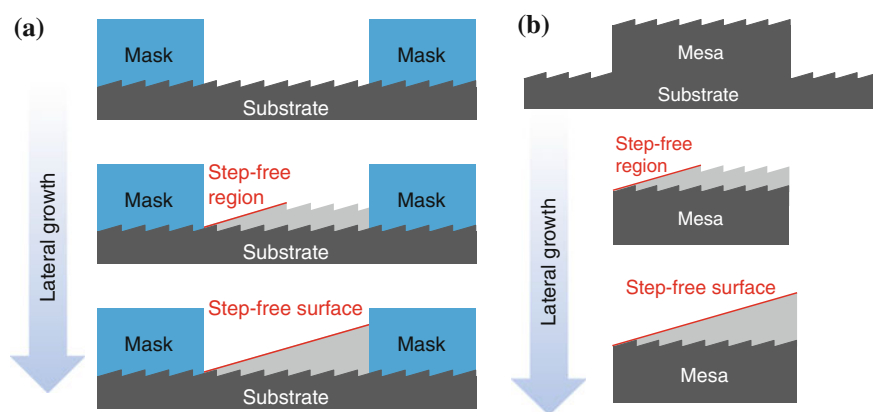


Fig. 1.15 Simplified models of step-free surface growth using **a** mask and **b** maskless processes. The step-free surfaces of GaAs and GaN were grown using the mask process, while Si, SiC, and diamond were grown using the maskless process

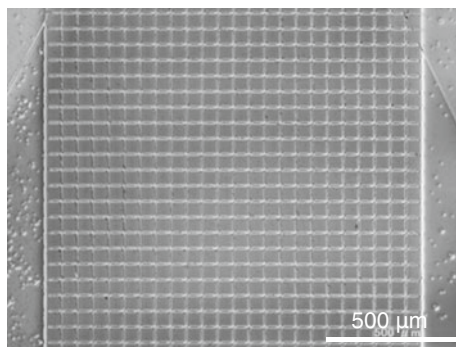


Fig. 1.16 OM image of single-crystal diamond substrates with $50 \times 50 \mu\text{m}^2$ mesas

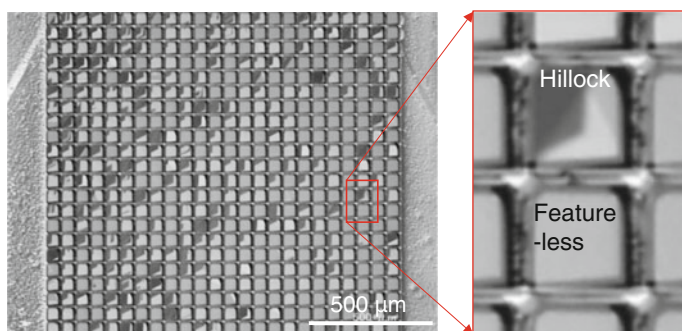


Fig. 1.17 OM image of diamond {111} films on single-crystal diamond substrates with $50 \times 50 \mu\text{m}^2$ mesas after homoepitaxial lateral growth

in which a mesa structure is used, is a maskless process. Method II should be utilized for diamond growth by PECVD because, in plasma environments, most materials do not meet the conditions necessary for the mask. Figure 1.16 shows an OM image of a {111} diamond substrate surface after mesa fabrication. The array formation of $50 \times 50 \mu\text{m}^2$ mesas on single-crystal diamond substrates was carried out through a conventional lithographic technique. Figure 1.17 shows an OM image of a diamond {111} surface after homoepitaxial lateral growth by MPCVD. The mesas exhibit one of the following two characteristics in the OM observations shown in Fig. 1.17: (1) the surface was featureless; or (2) the surface contained at least one hillock, which grew spirally on the substrate, as shown in Fig. 1.10. The hillock was induced by a screw dislocation, as shown in Fig. 1.18 [114, 146]. The featureless mesa surface is an atomically step-free surface, as shown in Fig. 1.19a. Additionally, the diamond {111} films with step-free surfaces contained no dislocations, as shown in Fig. 1.20. Recently, the growth of a $100 \times 100 \mu\text{m}^2$ step-free diamond {111} surface has been

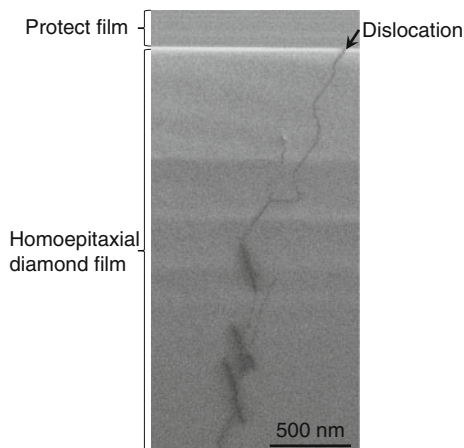


Fig. 1.18 Cross-sectional transmission electron microscope (XTEM) image of homoepitaxial diamond {111} film obtained from the mesa with hillock

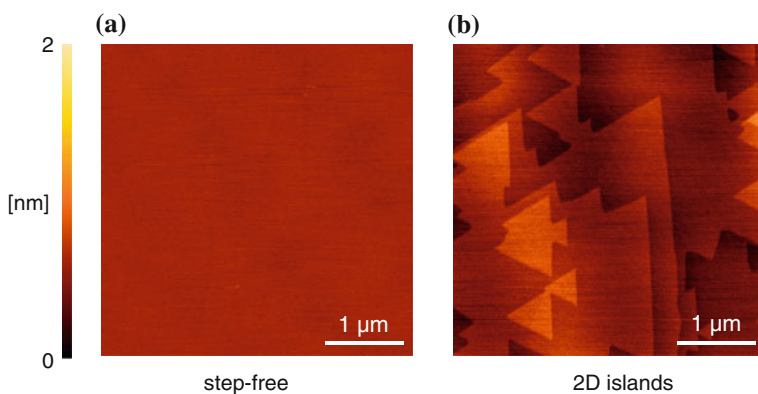


Fig. 1.19 AFM images of **a** atomically step-free diamond {111} surface and **b** atomically flat diamond {111} surface with 2D islands. The 2D islands were composed of atomically flat surfaces and a single BL step

reported [113, 114]. This indicates the possibility of forming a step-free diamond surface over a substrate if the substrate contains no dislocation. The author is also sure that this growth technique will be a key to realize high-quality diamond wafers which will allow manufacturing high quality interfaces and devices, e.g. high power devices, deep ultra-violet light-emitting diodes, bio/chemical sensors, quantum devices, etc.

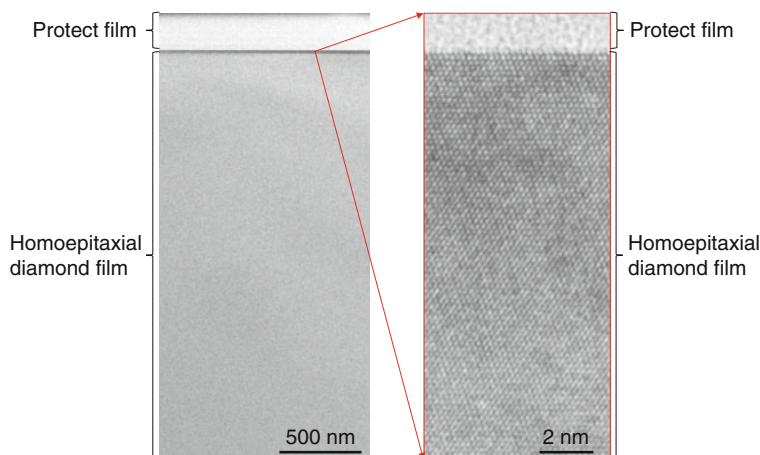


Fig. 1.20 XTEM images of homoepitaxial diamond {111} film obtained from featureless mesas

1.6 Conclusions

In this paper, the mechanism and control of homoepitaxial diamond growth by PECVD was reviewed. Recently, homoepitaxial diamond films have been used to fabricate many diamond devices. Judging from the reported performance of such devices, the technology of homoepitaxial diamond growth seems to have reached a certain level. However, because of the difficulty of in situ characterization in plasma environments, the growth mechanism remains unclear at present, especially regarding formation of precursors and their surface reactions. In the future, further developments of epitaxial diamond growth technology, including impurity doping and defect control, will be necessary to realize diamond-based electronics.

Acknowledgments The author sincerely thanks Prof. Satoshi Yamasaki, Dr. Hideyo Okushi, Dr. Daisuke Takeuchi, Dr. Masahiko Ogura, Dr. Toshiharu Makino, Dr. Hiromitsu Kato, Dr. Hitoshi Umezawa, Dr. Takehide Miyazaki of the National Institute of Advanced Industrial Science and Technology; Dr. Sung-Gi Ri of the National Institute for Materials Science; and Professor Takao Inokuma of Kanazawa University for fruitful discussions. This study was partly supported by a Grant-in-Aid for Young Scientists (A) (No. 24686074) from the Japan Society for the Promotion of Science, and Adaptable and Seamless Technology Transfer Program (A-STEP) and Core Research for Evolutional Science and Technology (CREST) from the Japan Science and Technology Agency.

References

1. B.V. Spitsyn, L.L. Bouilov, B.V. Derjaguin, Vapor growth of diamond on diamond and other surfaces. *J. Cryst. Growth* **52**(Part 1), 219–226 (1981). doi:[10.1016/0022-0248\(81\)90197-4](https://doi.org/10.1016/0022-0248(81)90197-4)
2. S. Matsumoto, Y. Sato, M. Kamo, N. Setaka, Vapor deposition of diamond particles from methane. *Jpn. J. Appl. Phys.* **21**(4, Part 2), L183–L185 (1982). doi:[10.1143/JJAP.21.L183](https://doi.org/10.1143/JJAP.21.L183)

3. M. Kamo, Y. Sato, S. Matsumoto, N. Setaka, Diamond synthesis from gas phase in microwave plasma. *J. Cryst. Growth* **62**(3), 642–644 (1983). doi:[10.1016/0022-0248\(83\)90411-6](https://doi.org/10.1016/0022-0248(83)90411-6)
4. M. Kamo, H. Yurimoto, Epitaxial growth of diamond on diamond substrate by plasma assisted CVD. *Appl. Surf. Sci.* **33–34**, 553–560 (1988). doi:[10.1016/0169-4332\(88\)90352-2](https://doi.org/10.1016/0169-4332(88)90352-2)
5. D.G. Goodwin, J.E. Butler, in *Handbook of Industrial Diamond and Diamond Films*, ed. by M.A. Prelas, G. Popovici, L.K. Biglow (Marcel Dekker, Inc., NY, 1997), p. 527
6. T. Teraji, in *Physics and Applications of CVD Diamond*, ed. by S. Koizumi, C.E. Nebel, M. Nesladek (Wiley-VCH Verlag GmbH & Co. KGaA, Weinheim, 2008), p. 29
7. J.E. Butler, A. Cheesman, M.N.R. Ashfold, in *CVD Diamond for Electronic Devices and Sensors*, ed. by R.S. Sussmann (Wiley, UK, 2009), p. 103
8. J.E. Butler, Y.A. Mankelevich, A. Cheesman, J. Ma, M.N.R. Ashfold, Understanding the chemical vapor deposition of diamond: recent progress. *J. Phys.: Cond. Mat.* **21**(5), 364201 (2009). doi:[10.1002/psa.200777501](https://doi.org/10.1002/psa.200777501)
9. O.A. Williams, R.B. Jackman, High growth rate MWPECVD of single crystal diamond. *Diam. Relat. Mater.* **13**(4–8), 557–560 (2004). doi:[10.1016/j.diamond.2004.01.023](https://doi.org/10.1016/j.diamond.2004.01.023)
10. J. Achard, F. Silva, O. Brinza, A. Tallaire, A. Gicquel, Coupled effect of nitrogen addition and surface temperature on the morphology and the kinetics of thick CVD diamond single crystals. *Diam. Relat. Mater.* **16**(4–7), 685–689 (2007). doi:[10.1016/j.diamond.2006.09.012](https://doi.org/10.1016/j.diamond.2006.09.012)
11. H. Yamada, A. Chayahara, Y. Mokuno, S. Shikata, Numerical and experimental studies of high growth-rate over area with 1-inch in diameter under moderate input-power by using MWPCVD. *Diam. Relat. Mater.* **17**(7–10), 1062 (2008). doi:[10.1016/j.diamond.2008.01.045](https://doi.org/10.1016/j.diamond.2008.01.045)
12. Q. Liang, C.Y. Chin, J. Lai, C. Yan, Y. Meng, H. Mao, R.J. Hemley, Enhanced growth of high quality single crystal diamond by microwave plasma assisted chemical vapor deposition at high gas pressures. *Appl. Phys. Lett.* **94**(2), 024103 (2009). doi:[10.1063/1.3072352](https://doi.org/10.1063/1.3072352)
13. Y. Gu, J. Lu, T. Grotjohn, T. Schuelke, J. Asmussen, Microwave plasma reactor design for high pressure and high power density diamond synthesis. *Diam. Relat. Mater.* **24**, 210–214 (2012). doi:[10.1016/j.diamond.2012.01.026](https://doi.org/10.1016/j.diamond.2012.01.026)
14. Y. Su, H.D. Li, S.H. Cheng, Q. Zhang, Q.L. Wang, X.Y. Lv, G.T. Zou, X.Q. Pei, J.G. Xie, Effect of N₂O on high-rate homoepitaxial growth of CVD single crystal diamonds. *J. Cryst. Growth* **351**(1), 51–55 (2012). doi:[10.1016/j.jcrysgro.2012.03.041](https://doi.org/10.1016/j.jcrysgro.2012.03.041)
15. J. Lu, Y. Gu, T.A. Grotjohn, T. Schuelke, J. Asmussen, Experimentally defining the safe and efficient, high pressure microwave plasma assisted CVD operating regime for single crystal diamond synthesis. *Diam. Relat. Mater.* **37**, 17–28 (2013). doi:[10.1016/j.diamond.2013.04.007](https://doi.org/10.1016/j.diamond.2013.04.007)
16. N. Fujimori, T. Imai, A. Doi, Characterization of conducting diamond films. *Vacuum* **36** (1–3), 99–102 (1986). doi:[10.1016/0042-207X\(86\)90279-4](https://doi.org/10.1016/0042-207X(86)90279-4)
17. N. Fujimori, H. Nakahata, T. Imai, Properties of boron-doped epitaxial diamond films. *Jpn. J. Appl. Phys.* **29**(5, Part 1), 824–827 (1990). doi:[10.1143/JJAP.29.824](https://doi.org/10.1143/JJAP.29.824)
18. S. Yamanaka, D. Takeuchi, H. Watanabe, H. Okushi, K. Kajimura, Low-compensated boron-doped homoepitaxial diamond films using trimethylboron. *Phys. Stat. Sol. A* **174**(1), 59–64 (1999). doi:[10.1002/\(SICI\)1521-396X\(199907\)174:1<59::AID-PSSA59>3.0.CO;2-A](https://doi.org/10.1002/(SICI)1521-396X(199907)174:1<59::AID-PSSA59>3.0.CO;2-A)
19. T. Tsubota, T. Fukui, M. Kameta, T. Saito, K. Kusakabe, S. Morooka, H. Maeda, Effect of total reaction pressure on electrical properties of boron doped homoepitaxial (100) diamond films formed by microwave plasma-assisted chemical vapor deposition using trimethylboron. *Diam. Relat. Mater.* **8**(6), 1079–1082 (1999). doi:[10.1016/S0925-9635\(99\)00096-5](https://doi.org/10.1016/S0925-9635(99)00096-5)
20. S. Ri, H. Kato, M. Ogura, H. Watanabe, T. Makino, S. Yamasaki, H. Okushi, Electrical and optical characterization of boron-doped (111) homoepitaxial diamond films. *Diam. Relat. Mater.* **14**(11–12), 1964–1968 (2005). doi:[10.1016/j.diamond.2005.06.032](https://doi.org/10.1016/j.diamond.2005.06.032)
21. C. Baron, M. Wade, A. Deneuville, F. Jomard, J. Chevallier, Cathodoluminescence of highly and heavily boron doped (100) homoepitaxial diamond films. *Diam. Relat. Mater.* **15**(4–8), 597–601 (2006). doi:[10.1016/j.diamond.2006.01.015](https://doi.org/10.1016/j.diamond.2006.01.015)
22. T. Teraji, H. Wada, M. Yamamoto, K. Arima, T. Ito, Highly efficient doping of boron into high-quality homoepitaxial diamond films. *Diam. Relat. Mater.* **15**(4–8), 602–606 (2006). doi:[10.1016/j.diamond.2006.01.011](https://doi.org/10.1016/j.diamond.2006.01.011)

23. T. Teraji, Chemical vapor deposition of homoeptaxial diamond films. *Phys. Stat. Sol. A* **203** (13), 3324–3357 (2006). doi:[10.1002/pssa.200671408](https://doi.org/10.1002/pssa.200671408)
24. V. Mortet, M. Daenen, T. Teraji, A. Lazea, V. Vorliceck, J. D’Haen, K. Haenen, M. D’Olieslaeger, Characterization of boron doped diamond epilayers grown in a NIRIM type reactor. *Diam. Relat. Mater.* **17**(7–10), 1330–1334 (2008). doi:[10.1016/j.diamond.2008.01.087](https://doi.org/10.1016/j.diamond.2008.01.087)
25. J. Barjon, N. Habka, C. Mer, F. Jormard, J. Chevallier, P. Bergonzo, Resistivity of boron doped diamond. *Phys. Stat. Sol. RRL* **3**(6), 202–204 (2009). doi:[10.1002/pssr.200903097](https://doi.org/10.1002/pssr.200903097)
26. J. Pernot, P.N. Volpe, F. Omnès, P. Muret, Hall hole mobility in boron-doped homoeptaxial diamond. *Phys. Rev. B* **81**(20), 205203 (2010). doi:[10.1103/PhysRevB.81.205203](https://doi.org/10.1103/PhysRevB.81.205203)
27. F. Omnès, P. Muret, P.N. Volpe, M. Wade, J. Pernot, F. Jomard, Study of boron doping in MPCVD grown homoeptaxial diamond layers based on cathodoluminescence spectroscopy, secondary ion mass spectroscopy and capacitance–voltage measurements. *Diam. Relat. Mater.* **20**(7), 912–916 (2011). doi:[10.1016/j.diamond.2011.05.010](https://doi.org/10.1016/j.diamond.2011.05.010)
28. M. Ogura, H. Kato, T. Makino, H. Okushi, S. Yamasaki, Misorientation-angle dependence of boron incorporation into (0 0 1)-oriented chemical-vapor-deposited (CVD) diamond. *J. Cryst. Growth* **317**(1), 60–63 (2011). doi:[10.1016/j.jcrysgro.2011.01.010](https://doi.org/10.1016/j.jcrysgro.2011.01.010)
29. M.E. Belousov, Y.A. Mankelevich, P.V. Minakov, A.T. Rakhimov, N.V. Suetin, R.A. Khmelnskiy, A.A. Tal, A.V. Khomich, Boron-doped homoeptaxial diamond CVD from microwave plasma-activated ethanol/trimethyl borate/hydrogen mixtures. *Chem. Vap. Depos.* **18**(10–12), 302–306 (2012). doi:[10.1002/cvde.201206993](https://doi.org/10.1002/cvde.201206993)
30. J. Achard, R. Issaoui, A. Tallaire, F. Silva, J. Barjon, F. Jomard, A. Gicquel, Freestanding CVD boron doped diamond single crystals: a substrate for vertical power electronic devices? *Phys. Stat. Sol. A* **209**(9), 1651–1658 (2012). doi:[10.1002/pssa.201200045](https://doi.org/10.1002/pssa.201200045)
31. A. Lazea, Y. Garino, T. Teraji, S. Koizumi, High quality p-type chemical vapor deposited {111}-oriented diamonds: growth and fabrication of related electrical devices. *Phys. Stat. Sol. A* **209**(10), 1978–1981 (2012). doi:[10.1002/pssa.201228162](https://doi.org/10.1002/pssa.201228162)
32. S. Koizumi, M. Kamo, Y. Sato, H. Ozaki, T. Inuzuka, Growth and characterization of phosphorous doped {111} homoeptaxial diamond thin films. *Appl. Phys. Lett.* **71**(8), 1065–1067 (1997). doi:[10.1063/1.119729](https://doi.org/10.1063/1.119729)
33. S. Koizumi, T. Teraji, H. Kanda, Phosphorus-doped chemical vapor deposition of diamond. *Diam. Relat. Mater.* **9**(3–6), 935–940 (2000). doi:[10.1016/S0925-9635\(00\)00217-X](https://doi.org/10.1016/S0925-9635(00)00217-X)
34. M. Katagiri, J. Isoya, S. Koizumi, H. Kanda, Lightly phosphorus-doped homoeptaxial diamond films grown by chemical vapor deposition. *Appl. Phys. Lett.* **85**(26), 6365–6367 (2004). doi:[10.1063/1.1840119](https://doi.org/10.1063/1.1840119)
35. M. Suzuki, H. Yoshida, N. Sakuma, T. Ono, T. Sakai, S. Koizumi, Electrical characterization of phosphorus-doped n-type homoeptaxial diamond layers by Schottky barrier diodes. *Appl. Phys. Lett.* **84**(13), 2349–2351 (2004). doi:[10.1063/1.1695206](https://doi.org/10.1063/1.1695206)
36. M. Suzuki, S. Koizumi, M. Katagiri, H. Yoshida, N. Sakuma, T. Ono, T. Sakai, Electrical characterization of phosphorus-doped n-type homoeptaxial diamond layers. *Diam. Relat. Mater.* **13**(11–12), 2037–2040 (2004). doi:[10.1016/j.diamond.2004.06.022](https://doi.org/10.1016/j.diamond.2004.06.022)
37. H. Kato, S. Yamasaki, H. Okushi, n-Type doping of (001)-oriented single-crystalline diamond by phosphorus. *Appl. Phys. Lett.* **86**(22), 222111 (2005). doi:[10.1063/1.1944228](https://doi.org/10.1063/1.1944228)
38. S. Koizumi, M. Suzuki, n-Type doping of diamond. *Phys. Stat. Sol. A* **203**(13), 3358–3366 (2006). doi:[10.1002/pssa.200671407](https://doi.org/10.1002/pssa.200671407)
39. H. Kato, T. Makino, S. Yamasaki, H. Okushi, n-Type diamond growth by phosphorus doping on (001)-oriented surface. *J. Phys. D Appl. Phys.* **40**(20), 6189–6200 (2007). doi:[10.1088/0022-3727/40/20/s05](https://doi.org/10.1088/0022-3727/40/20/s05)
40. J. Perot, S. Koizumi, Electron mobility in phosphorous doped {111} homoeptaxial diamond. *Appl. Phys. Lett.* **93**(5), 052105 (2008). doi:[10.1063/1.2969066](https://doi.org/10.1063/1.2969066)
41. H. Kato, D. Takeuchi, N. Tokuda, H. Umezawa, S. Yamasaki, H. Okushi, Electrical activity of doped phosphorus atoms in (001) n-type diamond. *Phys. Stat. Sol. A* **205**(9), 2195–2199 (2008). doi:[10.1002/pssa.200879722](https://doi.org/10.1002/pssa.200879722)

42. M.-A. Pinault-Thaury, B. Berini, I. Sternger, E. Chikoidze, A. Lusson, F. Jomard, J. Chevallier, J. Barjon, High fraction of substitutional phosphorus in a (100) diamond epilayer with low surface roughness. *Appl. Phys. Lett.* **100**(19), 192109 (2012). doi:[10.1063/1.4712617](https://doi.org/10.1063/1.4712617)
43. S. Koizumi, K. Watanabe, M. Hasegawa, H. Kanda, Ultraviolet emission from a diamond pn junction. *Science* **292**(5523), 1899–1901 (2001). doi:[10.1126/science.1060258](https://doi.org/10.1126/science.1060258)
44. H. Okushi, High quality homoepitaxial CVD diamond for electronic devices. *Diam. Relat. Mater.* **10**(3–7), 281–288 (2001). doi:[10.1016/S0925-9635\(00\)00399-X](https://doi.org/10.1016/S0925-9635(00)00399-X)
45. T. Makino, N. Tokuda, H. Kato, M. Ogura, H. Watanabe, S. Ri, S. Yamasaki, H. Okushi, High-efficiency excitonic emission with deep-ultraviolet light from (001)-oriented diamond p-i-n junction. *Jpn. J. Appl. Phys.* **45**(37–41, Part 2), L1042–L1044 (2006). doi:[10.1143/jjap.45.11042](https://doi.org/10.1143/jjap.45.11042)
46. D. Shin, N. Tokuda, B. Rezek, C.E. Nebel, Periodically arranged benzene-linker molecules on boron-doped single-crystalline diamond films for DNA sensing. *Electrochem. Commun.* **8** (5), 844–850 (2006). doi:[10.1016/j.elecom.2006.03.014](https://doi.org/10.1016/j.elecom.2006.03.014)
47. D. Shin, B. Rezek, N. Tokuda, D. Takeuchi, H. Watanabe, T. Nakamura, T. Yamamoto, C.E. Nebel, Photo- and electrochemical bonding of DNA to single crystalline CVD diamond. *Phys. Stat. Sol. A* **203**(13), 3245–3272 (2006). doi:[10.1002/pssa.200671402](https://doi.org/10.1002/pssa.200671402)
48. H. Umezawa, N. Tokuda, M. Ogura, S. Ri, S. Shikata, Characterization of leakage current on diamond Schottky barrier diodes using thermionic-field emission modeling. *Diam. Relat. Mater.* **15**(11–12), 1949–1953 (2006). doi:[10.1016/j.diamond.2006.08.030](https://doi.org/10.1016/j.diamond.2006.08.030)
49. K.-S. Song, T. Hiraki, H. Umezawa, H. Kawarada, Miniaturized diamond field-effect transistors for application in biosensors in electrolyte solution. *Appl. Phys. Lett.* **90**(6), 063901 (2007). doi:[10.1063/1.2454390](https://doi.org/10.1063/1.2454390)
50. E. Kohn, A. Denisenko, Concepts for diamond electronics. *Thin Solid Films* **515**(10), 4333–4339 (2007). doi:[10.1016/j.tsf.2006.07.179](https://doi.org/10.1016/j.tsf.2006.07.179)
51. M. Liao, Y. Koide, J. Alvarez, Single Schottky-barrier photodiode with interdigitated-finger geometry: application to diamond. *Appl. Phys. Lett.* **90**(12), 123507 (2007). doi:[10.1063/1.2715440](https://doi.org/10.1063/1.2715440)
52. T. Makino, N. Tokuda, H. Kato, M. Ogura, H. Watanabe, S. Ri, S. Yamasaki, H. Okushi, Electrical and light-emitting properties of (001)-oriented homoepitaxial diamond p-i-n junction. *Diam. Relat. Mater.* **16**(4–7), 1025–1028 (2007). doi:[10.1016/j.diamond.2007.01.024](https://doi.org/10.1016/j.diamond.2007.01.024)
53. C.E. Nebel, D. Shin, B. Rezek, N. Tokuda, H. Uetsuka, H. Watanabe, Diamond and biology. *J. R. Soc. Interface* **4**(14), 439–461 (2007). doi:[10.1098/rsif.2006.0196](https://doi.org/10.1098/rsif.2006.0196)
54. H. Umezawa, T. Saito, N. Tokuda, M. Ogura, S. Ri, H. Yoshikawa, S. Shikata, Leakage current analysis of diamond Schottky barrier diode. *Appl. Phys. Lett.* **90**(7), 073506 (2007). doi:[10.1063/1.2643374](https://doi.org/10.1063/1.2643374)
55. T. Makino, N. Tokuda, H. Kato, S. Kanno, S. Yamasaki, H. Okushi, Electrical and light-emitting properties of homoepitaxial diamond p-i-n junction. *Phys. Stat. Sol. A* **205**(9), 2200–2206 (2008). doi:[10.1002/pssa.200879717](https://doi.org/10.1002/pssa.200879717)
56. T. Makino, S. Tanimoto, Y. Hayashi, H. Kato, N. Tokuda, M. Ogura, D. Takeuchi, K. Oyama, H. Ohashi, H. Okushi, S. Yamasaki, Diamond Schottky-pn diode with high forward current density and fast switching operation. *Appl. Phys. Lett.* **94**(26), 262101 (2009). doi:[10.1063/1.3159837](https://doi.org/10.1063/1.3159837)
57. T. Makino, S. Ri, N. Tokuda, H. Kato, S. Yamasaki, H. Okushi, Electrical and light-emitting properties from (111)-oriented homoepitaxial diamond p-i-n junctions. *Diam. Relat. Mater.* **18**(5–8), 764–767 (2009). doi:[10.1016/j.diamond.2009.01.016](https://doi.org/10.1016/j.diamond.2009.01.016)
58. K. Oyama, S. Ri, H. Kato, M. Ogura, T. Makino, D. Takeuchi, N. Tokuda, H. Okushi, S. Yamasaki, High performance of diamond p⁺-i-n⁺ junction diode fabricated using heavily doped p⁺ and n⁺ layers. *Appl. Phys. Lett.* **94**(15), 152109 (2009). doi:[10.1063/1.3120560](https://doi.org/10.1063/1.3120560)
59. P.-N. Volpe, P. Muret, J. Pernot, F. Omnès, T. Teraji, Y. Koide, F. Jomard, D. Planson, P. Brosselard, N. Dheilily, B. Vergne, S. Scharnholtz, Extreme dielectric strength in boron doped homoepitaxial diamond. *Appl. Phys. Lett.* **97**(22), 223501 (2010). doi:[10.1063/1.3520140](https://doi.org/10.1063/1.3520140)

60. R. Hoffmann, A. Kriele, H. Obloh, N. Tokuda, W. Smirnov, N. Yang, C.E. Nebel, The creation of a biomimetic interface between boron-doped diamond and immobilized proteins. *Biomaterials* **32**(30), 7325–7332 (2011). doi:[10.1016/j.biomaterials.2011.06.052](https://doi.org/10.1016/j.biomaterials.2011.06.052)
61. T. Kawae, Y. Hori, T. Nakajima, H. Kawasaki, N. Tokuda, S. Okamura, Y. Takano, A. Morimoto, Structure and electrical properties of (Pr, Mn)-codoped BiFeO₃/B-doped diamond layered structure. *Electrochem. Solid-State Lett.* **14**(6), G31–G34 (2011). doi:[10.1149/1.3568838](https://doi.org/10.1149/1.3568838)
62. H. Kwarada, A.R. Ruslinda, Diamond electrolyte solution gate FETs for DNA and protein sensors using DNA/RNA aptamers. *Phys. Stat. Sol. A* **208**(9), 2005–2016 (2011). doi:[10.1002/pssa.201100503](https://doi.org/10.1002/pssa.201100503)
63. R. Hoffmann, H. Obloh, N. Tokuda, N. Yang, C.E. Nebel, Fractional surface termination of diamond by electrochemical oxidation. *Langmuir* **28**(1), 47–50 (2012). doi:[10.1021/la2039366](https://doi.org/10.1021/la2039366)
64. T. Iwasaki, Y. Hoshino, K. Tsuzuki, H. Kato, T. Makino, M. Ogura, D. Takeuchi, T. Matsumoto, H. Okushi, S. Yamasaki, M. Hatano, Diamond junction field-effect transistors with selectively grown n+-side gates. *Appl. Phys. Express* **5**(9), 091301 (2012). doi:[10.1143/apex.5.091301](https://doi.org/10.1143/apex.5.091301)
65. H. Kato, K. Oyama, T. Makino, M. Ogura, D. Takeuchi, S. Yamasaki, Diamond bipolar junction transistor device with phosphorus-doped diamond base layer. *Diam. Relat. Mater.* **27–28**, 19–22 (2012). doi:[10.1016/j.diamond.2012.05.004](https://doi.org/10.1016/j.diamond.2012.05.004)
66. T. Kawae, H. Kawasaki, T. Nakajima, N. Tokuda, S. Okamura, A. Morimoto, Y. Takano, A. Morimoto, Y. Takano, Fabrication of (Bi,Pr)(Fe,Mn)O₃ thin films on polycrystalline diamond substrates by chemical solution deposition and their properties. *Jpn. J. Appl. Phys.* **51**(9 S1), 09LA08 (2012). doi:[10.1143/jjap.51.09la08](https://doi.org/10.1143/jjap.51.09la08)
67. R. Edgington, A.R. Ruslinda, S. Sato, Y. Ishiyama, K. Tsuge, T. Ono, H. Kwarada, R.B. Jackman, Boron delta-doped (111) diamond solution gate field effect transistors. *Biosens. Bioelectron.* **33**(1), 152–157 (2012). doi:[10.1016/j.bios.2011.12.044](https://doi.org/10.1016/j.bios.2011.12.044)
68. H. Kwarada, High-current metal oxide semiconductor field-effect transistors on H-terminated diamond surfaces and their high-frequency operation. *Jpn. J. Appl. Phys.* **51**(9R), 090111 (2012). doi:[10.1143/jjap.51.090111](https://doi.org/10.1143/jjap.51.090111)
69. T. Makino, H. Kato, D. Takeuchi, M. Ogura, H. Okushi, S. Yamasaki, Device design of diamond Schottky-pn diode for low-loss power electronics. *Jpn. J. Appl. Phys.* **51**(9R), 090116 (2012). doi:[10.1143/jjap.51.090116](https://doi.org/10.1143/jjap.51.090116)
70. S. Cheng, L. Sang, M. Liao, J. Liu, M. Imura, H. Li, Y. Koide, Integration of high-dielectric constant Ta₂O₅ oxides on diamond for power devices. *Appl. Phys. Lett.* **101**(23), 232907 (2012). doi:[10.1063/1.4770059](https://doi.org/10.1063/1.4770059)
71. N. Mizuochi, T. Makino, H. Kato, D. Takeuchi, M. Ogura, H. Okushi, M. Nothaft, P. Neumann, A. Gali, F. Jelezko, J. Wrachtrup, S. Yamasaki, Electrically driven single-photon source at room temperature in diamond. *Nat. Photon.* **6**, 299–303 (2012). doi:[10.1038/nphoton.2012.75](https://doi.org/10.1038/nphoton.2012.75)
72. M. Liao, L. Sang, T. Teraji, M. Imura, J. Alvarez, Y. Koide, Comprehensive investigation of single crystal diamond deep-ultraviolet detectors. *Jpn. J. Appl. Phys.* **51**(9R), 090115 (2012). doi:[10.1143/jjap.51.090115](https://doi.org/10.1143/jjap.51.090115)
73. D. Takeuchi, T. Makino, H. Kato, M. Ogura, H. Okushi, H. Ohashi, S. Yamasaki, High-voltage vacuum switch with a diamond p–i–n diode using negative electron affinity. *Jpn. J. Appl. Phys.* **51**(9R), 090113 (2012). doi:[10.1143/jjap.51.090113](https://doi.org/10.1143/jjap.51.090113)
74. H. Umezawa, M. Nagase, Y. Kato, S. Shikata, High temperature application of diamond power device. *Diam. Relat. Mater.* **24**, 201–205 (2012). doi:[10.1016/j.diamond.2012.01.011](https://doi.org/10.1016/j.diamond.2012.01.011)
75. G. Chicot, A. Maréchal, R. Motte, P. Muret, E. Gheeraert, J. Pernot, Metal oxide semiconductor structure using oxygen-terminated diamond. *Appl. Phys. Lett.* **102**(24), 242108 (2013). doi:[10.1063/1.4811668](https://doi.org/10.1063/1.4811668)
76. A. Gicquel, K. Hassouni, S. Farhat, Y. Breton, C.D. Scott, M. Lefebvre, M. Pealat, Spectroscopic analysis and chemical kinetics modeling of a diamond deposition plasma reactor. *Diam. Relat. Mater.* **3**(4–6), 581–586 (1994). doi:[10.1016/0925-9635\(94\)90229-1](https://doi.org/10.1016/0925-9635(94)90229-1)

77. C. Benndorf, P. Joeris, R. Kröger, Mass and optical emission spectroscopy of plasmas for diamond synthesis. *Pure Appl. Chem.* **66**(6), 1195–1205 (1994). doi:[10.1351/pac199466061195](https://doi.org/10.1351/pac199466061195)
78. T. Fujii, M. Kareev, Mass spectrometric studies of a CH₄/H₂ microwave plasma under diamond deposition conditions. *J. Appl. Phys.* **89**(5), 2543–2546 (2001). doi:[10.1063/1.1346655](https://doi.org/10.1063/1.1346655)
79. P. Deák, A. Kováts, P. Csikváry, I. Maros, G. Hárs, Ethynyl (C₂H): a major player in the chemical vapor deposition of diamond. *Appl. Phys. Lett.* **90**(5), 051503 (2007). doi:[10.1063/1.2437718](https://doi.org/10.1063/1.2437718)
80. H. Zhou, J. Watanabe, M. Miyake, A. Ogino, M. Nagatsu, R. Zhan, Optical and mass spectroscopy measurements of Ar/CH₄/H₂ microwave plasma for nano-crystalline diamond film deposition. *Diam. Relat. Mater.* **16**(4–7), 675–678 (2007). doi:[10.1016/j.diamond.2006.11.074](https://doi.org/10.1016/j.diamond.2006.11.074)
81. J. Ma, M.N.R. Ashfold, Y.A. Mankelevich, Validating optical emission spectroscopy as a diagnostic of microwave activated CH₄/Ar/H₂ plasmas used for diamond chemical vapor deposition. *J. Appl. Phys.* **105**(4), 043302 (2009). doi:[10.1063/1.3078032](https://doi.org/10.1063/1.3078032)
82. A. Gicquel, N. Derkaoui, C. Rond, F. Benedic, G. Cicala, D. Moneger, K. Hassouni, Quantitative analysis of diamond deposition reactor efficiency. *Chem. Phys.* **398**, 239–247 (2012). doi:[10.1016/j.chemphys.2011.08.022](https://doi.org/10.1016/j.chemphys.2011.08.022)
83. J.C. Richley, M.W. Kelly, M.N.R. Ashfold, Y.A. Mankelevich, Optical emission from microwave activated C/H/O gas mixtures for diamond chemical vapor deposition. *J. Phys. Chem. A* **116**(38), 9447–9458 (2012). doi:[10.1021/jp306191y](https://doi.org/10.1021/jp306191y)
84. P. Bou, J.C. Boettner, L. Vandenbulcke, Kinetic calculations in plasmas used for diamond deposition. *Jpn. J. Appl. Phys.* **31**(5A, Part 1), 1505–1513 (1992). doi:[10.1143/JJAP.31.1505](https://doi.org/10.1143/JJAP.31.1505)
85. M.C. McMaster, W.L. Hsu, M.E. Coltrin, D.S. Dandy, C. Fox, Dependence of the gas composition in a microwave plasma-assisted diamond chemical vapor deposition reactor on the inlet carbon source: CH₄ versus C₂H₂. *Diam. Relat. Mater.* **4**(7), 1000–1008 (1995). doi:[10.1016/0925-9635\(95\)00270-7](https://doi.org/10.1016/0925-9635(95)00270-7)
86. J.M. Larson, M.T. Swihart, S.L. Girshick, Characterization of the near-surface gas-phase chemical environment in atmospheric-pressure plasma chemical vapor deposition of diamond. *Diam. Relat. Mater.* **8**(10), 1863–1874 (1999). doi:[10.1016/S0925-9635\(99\)00143-0](https://doi.org/10.1016/S0925-9635(99)00143-0)
87. O. Aubry, J.-L. Delfau, C. Met, L. Vandenbulcke, C. Vovelle, Precursors of diamond films analysed by molecular beam mass spectrometry of microwave plasmas. *Diam. Relat. Mater.* **13**(1), 116–124 (2004). doi:[10.1016/j.diamond.2003.09.009](https://doi.org/10.1016/j.diamond.2003.09.009)
88. J. Achard, F. Silva, A. Tallaie, X. Bonnin, G. Lomvardi, K. Hassouni, A. Gicquel, High quality MPACVD diamond single crystal growth: high microwave power density regime. *J. Phys. D* **40**(20), 6175–6188 (2007). doi:[10.1088/0022-3727/40/20/S04](https://doi.org/10.1088/0022-3727/40/20/S04)
89. H. Yamada, A. Chayahara, Y. Mokuno, Simplified description of microwave plasma discharge for chemical vapor deposition of diamond. *J. Appl. Phys.* **101**(6), 063302 (2007). doi:[10.1063/1.2711811](https://doi.org/10.1063/1.2711811)
90. J. Ma, J.C. Richley, M.N.R. Ashfold, Y.A. Mankelevich, Probing the plasma chemistry in a microwave reactor used for diamond chemical vapor deposition by cavity ring down spectroscopy. *J. Appl. Phys.* **104**(10), 103305 (2008). doi:[10.1063/1.3021095](https://doi.org/10.1063/1.3021095)
91. F. Silva, J. Achard, O. Brinza, X. Bonnin, K. Hassouni, A. Anthonis, K.D. Corte, J. Barjon, High quality, large surface area, homoepitaxial MPACVD diamond growth. *Diam. Relat. Mater.* **18**(5–8), 683–697 (2009). doi:[10.1016/j.diamond.2009.01.038](https://doi.org/10.1016/j.diamond.2009.01.038)
92. K. Hassouni, F. Silva, A. Gicquel, Modelling of diamond deposition microwave cavity generated plasmas. *J. Phys. D* **43**(15), 153001 (2010). doi:[10.1088/0022-3727/43/15/153001](https://doi.org/10.1088/0022-3727/43/15/153001)
93. H. Yamada, A. Chayahara, Y. Mokuno, S. Shikata, Model of reactive microwave plasma discharge for growth of single-crystal diamond. *Jpn. J. Appl. Phys.* **50**(1S1), 01AB02 (2011). doi:[10.1143/jjap.50.01ab02](https://doi.org/10.1143/jjap.50.01ab02)
94. H. Yamada, Numerical simulations to study growth of single-crystal diamond by using microwave plasma chemical vapor deposition with reactive (H, C, N) species. *Jpn. J. Appl. Phys.* **51**(9R), 090105 (2012). doi:[10.1143/jjap.51.090105](https://doi.org/10.1143/jjap.51.090105)

95. C.-L. Cheng, H.-C. Chang, J.-C. Lin, K.-J. Song, J.-K. Wang, Direct observation of hydrogen etching anisotropy on diamond single crystal surfaces. *Phys. Rev. Lett.* **78**(19), 3713–3716 (1997). doi:[10.1103/PhysRevLett.78.3713](https://doi.org/10.1103/PhysRevLett.78.3713)
96. T. Tsuno, T. Imai, Y. Nishibayashi, K. Hamada, N. Fujimori, Epitaxially grown diamond (001) $2\times 1\times 2$ surface investigated by scanning tunneling microscopy in air. *Jpn. J. Appl. Phys.* **30**(5, Part 1), 1063–1066 (1991). doi:[10.1143/JJAP.30.1063](https://doi.org/10.1143/JJAP.30.1063)
97. H. Sasaki, H. Kawarada, Structure of chemical vapor deposited diamond (111) surfaces by scanning tunneling microscopy. *Jpn. J. Appl. Phys.* **32**(12A, Part 2), L1771–L1774 (1993). doi:[10.1143/JJAP.32.L1771](https://doi.org/10.1143/JJAP.32.L1771)
98. L.F. Sutcu, C.J. Chu, M.S. Thompson, R.H. Hauge, J.L. Margrave, M.P. D'Evelyn, Atomic force microscopy of (100), (110), and (111) homoepitaxial diamond films. *J. Appl. Phys.* **71**(12), 5930–5940 (1992). doi:[10.1063/1.350443](https://doi.org/10.1063/1.350443)
99. T. Tsuno, T. Tomikawa, S. Shikata, T. Imai, N. Fujimori, Diamond(001) single-domain 2×1 surface grown by chemical vapor deposition. *Appl. Phys. Lett.* **64**(5), 572–574 (1994). doi:[10.1063/1.111107](https://doi.org/10.1063/1.111107)
100. T. Tsuno, T. Tomikawa, S. Shikata, N. Fujimori, Diamond homoepitaxial growth on (111) substrate investigated by scanning tunneling microscope. *J. Appl. Phys.* **75**(3), 1526–1529 (1994). doi:[10.1063/1.356389](https://doi.org/10.1063/1.356389)
101. M. McGonigal, J.N. Russell Jr., P.E. Pehrsson, H.G. Maguire, J.E. Butler, Multiple internal reflection infrared spectroscopy of hydrogen adsorbed on diamond(110). *J. Appl. Phys.* **77**(8), 4049–4053 (1995). doi:[10.1063/1.359487](https://doi.org/10.1063/1.359487)
102. H. Kawarada, H. Ssaki, A. Sato, Scanning-tunneling-microscope observation of the homoepitaxial diamond (001) 2×1 reconstruction observed under atmospheric pressure. *Phys. Rev. B* **52**(15), 11351–11358 (1995). doi:[10.1103/PhysRevB.52.11351](https://doi.org/10.1103/PhysRevB.52.11351)
103. Y. Kuang, Y. Wang, N. Lee, A. Badzian, T. Badzian, T.T. Tsong, Surface structure of homoepitaxial diamond (001) films, a scanning tunneling microscopy study. *Appl. Phys. Lett.* **67**(25), 3721–3723 (1995). doi:[10.1063/1.115361](https://doi.org/10.1063/1.115361)
104. C.-L. Cheng, J.-C. Lin, H.-C. Chang, J.-K. Wang, Characterization of CH stretches on diamond C(111) single and nanocrystal surfaces by infrared absorption spectroscopy. *J. Chem. Phys.* **105**(19), 8977–8978 (1996). doi:[10.1063/1.472938](https://doi.org/10.1063/1.472938)
105. T. Takami, K. Suzuki, I. Kusunoki, I. Sakaguchi, M. Nishitani-Gamo, T. Ando, RHEED and AFM studies of homoepitaxial diamond thin film on C(001) substrate produced by microwave plasma CVD. *Diam. Relat. Mater.* **8**(2–5), 701–704 (1999). doi:[10.1016/S0925-9635\(98\)00391-4](https://doi.org/10.1016/S0925-9635(98)00391-4)
106. T. Takami, I. Kusunoki, M. Nishitani-Gamo, T. Ando, Homoepitaxial diamond (001) thin film studied by reflection high-energy electron diffraction, contact atomic force microscopy, and scanning tunneling microscopy. *J. Vac. Sci. Technol. B* **18**(3), 1198–1202 (2000). doi:[10.1116/1.591360](https://doi.org/10.1116/1.591360)
107. A. Heerwagen, M. Strobel, M. Himmelhaus, M. Buck, Chemical vapor deposition of diamond: an in situ study by vibrational spectroscopy. *J. Am. Chem. Soc.* **123**(27), 6732–6733 (2001). doi:[10.1021/ja016056q](https://doi.org/10.1021/ja016056q)
108. L.K. Bigelow, M.P. D'Evelyn, Role of surface and interface science in chemical vapor deposition diamond technology. *Surf. Sci.* **500**(1–3), 986–1004 (2002). doi:[10.1016/S0039-6028\(01\)01545-X](https://doi.org/10.1016/S0039-6028(01)01545-X)
109. L. Ackermann, W. Kulisch, Investigation of diamond etching and growth by in situ scanning tunneling microscopy. *Diam. Relat. Mater.* **8**(7), 1256–1260 (1999). doi:[10.1016/S0925-9635\(99\)00119-3](https://doi.org/10.1016/S0925-9635(99)00119-3)
110. B. Voigtländer, M. Kästner, P. Šmilauer, Magic islands in Si/Si(111) homoepitaxy. *Phys. Rev. Lett.* **81**(4), 858–861 (1998). doi:[10.1103/PhysRevLett.81.858](https://doi.org/10.1103/PhysRevLett.81.858)
111. H. Yamaguchi, Y. Homma, Imaging of layer by layer growth processes during molecular beam epitaxy of GaAs on (111)A substrates by scanning electron microscopy. *Appl. Phys. Lett.* **73**(21), 3079–3081 (1998). doi:[10.1063/1.122678](https://doi.org/10.1063/1.122678)

112. M.H. Xie, S.M. Seutter, W.K. Zhu, L.X. Zheng, H. Wu, S.Y. Tong, Anisotropic step-flow growth and island growth of GaN(0001) by molecular beam epitaxy. *Phys. Rev. Lett.* **82**(13), 2749–2752 (1999). doi:[10.1103/PhysRevLett.82.2749](https://doi.org/10.1103/PhysRevLett.82.2749)
113. N. Tokuda, T. Makino, T. Inokuma, S. Yamasaki, Formation of step-free surfaces on diamond (111) mesas by homoepitaxial lateral growth. *Jpn. J. Appl. Phys.* **51**(9R), 090107 (2012). doi:[10.1143/JJAP.51.090107](https://doi.org/10.1143/JJAP.51.090107)
114. N. Tokuda, T. Makino, T. Inokuma, S. Yamasaki, Formation of step-free diamond (111) surfaces by plasma-enhanced CVD. *J. Jpn. Assoc. Cryst. Growth* **39**(4), 185–189 (2012) (in Japanese)
115. F. Jelezko, T. Gaebel, I. Popa, A. Gruber, J. Wrachtrup, Observation of coherent oscillations in a single electron spin. *Phys. Rev. Lett.* **92**(7), 076401 (2004). doi:[10.1103/PhysRevLett.92.076401](https://doi.org/10.1103/PhysRevLett.92.076401)
116. L. Childress, M.V. Gurudev Dutt, J.M. Taylor, A.S. Zibrov, F. Jelezko, J. Wrachtrup, P.R. Hemmer, M.D. Lukin, Coherent dynamics of coupled electron and nuclear spin qubits in diamond. *Science* **314**(5797), 281–285 (2006). doi:[10.1126/science.1131871](https://doi.org/10.1126/science.1131871)
117. M.V. Gurudev Dutt, L. Childress, L. Jiang, E. Togan, J. Maze, F. Jelezko, A.S. Zibrov, P.R. Hemmer, M.D. Lukin, Quantum register based on individual electronic and nuclear spin qubits in diamond. *Science* **316**(5829), 1312–1316 (2007). doi:[10.1126/science.1139831](https://doi.org/10.1126/science.1139831)
118. J.R. Maze, J.M. Taylor, M.D. Lukin, Electron spin decoherence of single nitrogen-vacancy defects in diamond. *Phys. Rev. B* **78**(9), 094303 (2008). doi:[10.1103/PhysRevB.78.094303](https://doi.org/10.1103/PhysRevB.78.094303)
119. P. Neumann, N. Mizuochi, F. Rempp, P. Hemmer, H. Watanabe, S. Yamasaki, V. Jacques, T. Gaebel, F. Jelezko, J. Wrachtrup, Multipartite entanglement among single spins in diamond. *Science* **320**(5881), 1326–1329 (2008). doi:[10.1126/science.1157233](https://doi.org/10.1126/science.1157233)
120. G. Balasubramanian, P. Neumann, D. Twitchen, M. Markham, R. Kolesov, N. Mizuochi, J. Isoya, J. Achard, J. Beck, J. Tissler, V. Jacques, P.R. Hemmer, F. Jelezko, J. Wrachtrup, Ultralong spin coherence time in isotopically engineered diamond. *Nat. Mater.* **8**, 383–387 (2009). doi:[10.1038/nmat2420](https://doi.org/10.1038/nmat2420)
121. B.B. Buckley, G.D. Fuchs, L.C. Bassett, D.D. Awschalom, Spin-light coherence for single-spin measurement and control in diamond. *Science* **330**(6008), 1212–1215 (2010). doi:[10.1126/science.1196436](https://doi.org/10.1126/science.1196436)
122. X. Zhu, S. Saito, A. Kemp, K. Kakuyanagi, S. Karimoto, H. Nakano, W.J. Munro, Y. Tokura, M.S. Everitt, K. Nemoto, M. Kasu, N. Mizuochi, K. Semba, Coherent coupling of a superconducting flux qubit to an electron spin ensemble in diamond. *Nature* **478**(7368), 221–224 (2011). doi:[10.1038/nature10462](https://doi.org/10.1038/nature10462)
123. K.C. Lee, M.R. Sprague, B.J. Sussman, J. Nunn, N.K. Langford, X.-M. Jin, T. Champion, P. Michelberger, K.F. Reim, D. England, D. Jaksch, I.A. Walmsley, Entangling macroscopic diamonds at room temperature. *Science* **334**(6060), 1253–1256 (2011). doi:[10.1126/science.1211914](https://doi.org/10.1126/science.1211914)
124. J.F. Prings, Activation of boron-dopant atoms in ion-implanted diamonds. *Phys. Rev. B* **38**(8), 5576–5584 (1988). doi:[10.1103/PhysRevB.38.5576](https://doi.org/10.1103/PhysRevB.38.5576)
125. C. Uzan-Saguy, R. Kalish, R. Walker, D.N. Jamieson, S. Prawer, Formation of delta-doped, buried conducting layers in diamond, by high-energy, B-ion implantation. *Diam. Relat. Mater.* **7**(10), 1429–1432 (1998). doi:[10.1016/S0925-9635\(98\)00231-3](https://doi.org/10.1016/S0925-9635(98)00231-3)
126. K. Ueda, M. Kasu, T. Makimoto, High-pressure and high-temperature annealing as an activation method for ion-implanted dopants in diamond. *Appl. Phys. Lett.* **90**(12), 122102 (2007). doi:[10.1063/1.2715034](https://doi.org/10.1063/1.2715034)
127. N. Tsubouchi, M. Ogura, Enhancement of dopant activation in B-implanted diamond by high-temperature annealing. *Jpn. J. Appl. Phys.* **47**(9R), 7047–7051 (2008). doi:[10.1143/JJAP.47.7047](https://doi.org/10.1143/JJAP.47.7047)
128. N. Tsubouchi, M. Ogura, N. Mizuochi, H. Watanabe, Electrical properties of a B doped layer in diamond formed by hot B implantation and high-temperature annealing. *Diam. Relat. Mater.* **18**(2–3), 128–131 (2009). doi:[10.1016/j.diamond.2008.09.013](https://doi.org/10.1016/j.diamond.2008.09.013)

129. A.K. Ratnikova, M.P. Dukhnovsky, Y.Y. Fedorov, V.E. Zemlyakov, A.B. Muchnikov, A.L. Vikharev, A.M. Gorbachev, D.B. Radishev, A.A. Altukhov, A.V. Mitenkin, Homoepitaxial single crystal diamond grown on natural diamond seeds (type IIa) with boron-implanted layer demonstrating the highest mobility of $1150 \text{ cm}^2/\text{V s}$ at 300 K for ion-implanted diamond. *Diam. Relat. Mater.* **20**(8), 1243–1245 (2011). doi:[10.1016/j.diamond.2011.07.007](https://doi.org/10.1016/j.diamond.2011.07.007)
130. V.S. Bormashov, S.A. Tarelkin, S.G. Buga, M.S. Kuznetsov, S.A. Terentiev, A.N. Semenov, V.D. Blank, Electrical properties of the high quality boron-doped synthetic single-crystal diamonds grown by the temperature gradient method. *Diam. Relat. Mater.* **35**, 19–23 (2013). doi:[10.1016/j.diamond.2013.02.011](https://doi.org/10.1016/j.diamond.2013.02.011)
131. S. Yamanaka, H. Watanabe, S. Masai, D. Takeuchi, H. Okushi, K. Kajimura, High-quality B-doped homoepitaxial diamond films using trimethylboron. *Jpn. J. Appl. Phys.* **37**(10A, Part 2), L1129–L1131 (1998). doi:[10.1143/JJAP.37.L1129](https://doi.org/10.1143/JJAP.37.L1129)
132. J.-P. Lagrange, A. Deneuville, E. Gheeraert, Activation energy in low compensated homoepitaxial boron-doped diamond films. *Diam. Relat. Mater.* **7**(9), 1390–1393 (1998). doi:[10.1016/S0925-9635\(98\)00225-8](https://doi.org/10.1016/S0925-9635(98)00225-8)
133. E.A. Ekimov, V.A. Sidrov, E.D. Bauer, N.N. Mel'nki, N.J. Curro, J.D. Thompson, S.M. Stishov, Superconductivity in diamond. *Nature* **428**(6982), 542–545 (2004). doi:[10.1038/nature02449](https://doi.org/10.1038/nature02449)
134. Y. Takano, M. Nagao, I. Sakaguchi, M. Tachiki, T. Hatano, K. Kobayashi, H. Umezawa, H. Kwarada, Superconductivity in diamond thin films well above liquid helium temperature. *Appl. Phys. Lett.* **85**(14), 2851–2853 (2004). doi:[10.1063/1.1802389](https://doi.org/10.1063/1.1802389)
135. T. Yokoya, T. Nakamura, T. Matsushita, T. Muro, Y. Takano, M. Nagao, T. Takenouchi, H. Kwarada, T. Oguchi, Origin of the metallic properties of heavily boron-doped superconducting diamond. *Nature* **438**(7068), 647–650 (2005). doi:[10.1038/nature04278](https://doi.org/10.1038/nature04278)
136. E. Bustarret, Superconducting diamond: an introduction. *Phys. Stat. Sol. A* **205**(5), 997–1008 (2008). doi:[10.1002/pssa.200777501](https://doi.org/10.1002/pssa.200777501)
137. T. Klein, P. Achatz, J. Kacmarcik, C. Marcenat, F. Gustafsson, J. Marcus, E. Bustarret, J. Pernot, F. Omnes, B.E. Sernelius, C. Persson, A. Silva, C. Cytermann, Metal-insulator transition and superconductivity in boron-doped diamond. *Phys. Rev. B* **75**(16), 165313 (2007). doi:[10.1103/PhysRevB.75.165313](https://doi.org/10.1103/PhysRevB.75.165313)
138. A. Kawano, H. Ishiwata, S. Iriyama, R. Okada, T. Yamaguchi, Y. Takano, H. Kwarada, Superconductor-to-insulator transition in boron-doped diamond films grown using chemical vapor deposition. *Phys. Rev. B* **82**(8), 085318 (2010). doi:[10.1103/PhysRevB.82.085318](https://doi.org/10.1103/PhysRevB.82.085318)
139. N. Tokuda, T. Saito, H. Umezawa, H. Okushi, S. Yamasaki, The role of boron atoms in heavily boron-doped semiconducting homoepitaxial diamond growth—study of surface morphology. *Diam. Relat. Mater.* **16**(2), 409–411 (2007). doi:[10.1016/j.diamond.2006.08.013](https://doi.org/10.1016/j.diamond.2006.08.013)
140. N. Tokuda, H. Umezawa, T. Saito, K. Yamabe, H. Okushi, S. Yamasaki, Surface roughening of diamond (001) films during homoepitaxial growth in heavy boron doping. *Diam. Relat. Mater.* **16**(4–7), 767–770 (2007). doi:[10.1016/j.diamond.2006.12.024](https://doi.org/10.1016/j.diamond.2006.12.024)
141. N. Tokuda, H. Umezawa, K. Yamabe, H. Okushi, S. Yamasaki, Hillock-free heavily boron-doped homoepitaxial diamond films on misoriented (001) substrates. *Jpn. J. Appl. Phys.* **46**(4A, Part 1), 1469–1470 (2007). doi:[10.1143/JJAP.46.1469](https://doi.org/10.1143/JJAP.46.1469)
142. H. Kato, D. Takeuchi, N. Tokuda, H. Umezawa, H. Okushi, S. Yamasaki, Characterization of specific contact resistance on heavily phosphorus-doped diamond films. *Diam. Relat. Mater.* **18**(5–8), 782–785 (2009). doi:[10.1016/j.diamond.2009.01.033](https://doi.org/10.1016/j.diamond.2009.01.033)
143. T. Yatsui, W. Nomura, M. Naruse, M. Ohtsu, Realization of an atomically flat surface of diamond using dressed photon-phonon etching. *J. Phys. D* **45**(47), 475302 (2012). doi:[10.1088/0022-3727/45/47/475302](https://doi.org/10.1088/0022-3727/45/47/475302)
144. A. Kubota, S. Fukuyama, Y. Ichimori, M. Touge, Surface smoothing of single-crystal diamond (100) substrate by polishing technique. *Diam. Relat. Mater.* **24**, 59–62 (2012). doi:[10.1016/j.diamond.2011.10.022](https://doi.org/10.1016/j.diamond.2011.10.022)

145. Y. Kato, H. Umezawa, S. Shikata, M. Touge, Effect of an ultraflat substrate on the epitaxial growth of chemical-vapor-deposited diamond. *Appl. Phys. Express* **6**(2), 025506 (2013). doi:[10.7567/APEX.6.025506](https://doi.org/10.7567/APEX.6.025506)
146. N. Tokuda, H. Umezawa, K. Yamabe, H. Okushi, S. Yamasaki, Growth of atomically step-free surface on diamond {111} mesas. *Diam. Relat. Mater.* **19**(4), 288–290 (2010). doi:[10.1016/j.diamond.2009.11.015](https://doi.org/10.1016/j.diamond.2009.11.015)
147. H. Sawada, H. Ichinose, H. Watanabe, D. Takeuchi, H. Okushi, Cross-sectional TEM study of unepitaxial crystallites in a homoepitaxial diamond film. *Diam. Relat. Mater.* **10**(11), 2030–2034 (2001). doi:[10.1016/S0925-9635\(01\)00477-0](https://doi.org/10.1016/S0925-9635(01)00477-0)
148. T. Tsuno, T. Imai, N. Fujimori, Twinning structure and growth hillock on diamond (001) epitaxial film. *Jpn. J. Appl. Phys.* **33**(7A, Part 1), 4039–4043 (1994). doi:[10.1143/JJAP.33.4039](https://doi.org/10.1143/JJAP.33.4039)
149. H. Wanatanbe, D. Takeuchi, S. Yamanaka, H. Okushi, K. Kajimura, T. Sekiguchi, Homoepitaxial diamond film with an atomically flat surface over a large area. *Diam. Relat. Mater.* **8**(7), 1272 (1999). doi:[10.1016/S0925-9635\(99\)00126-0](https://doi.org/10.1016/S0925-9635(99)00126-0)
150. N. Tokuda, H. Umezawa, S. Ri, M. Ogura, K. Yamabe, H. Okushi, S. Yamasaki, Atomically flat diamond (111) surface formation by homoepitaxial lateral growth. *Diam. Relat. Mater.* **17**(7–10), 1051–1054 (2008). doi:[10.1016/j.diamond.2008.01.089](https://doi.org/10.1016/j.diamond.2008.01.089)
151. N. Tokuda, H. Umezawa, H. Kato, M. Ogura, S. Gonda, K. Yamabe, H. Okushi, S. Yamasaki, Nanometer scale height standard using atomically controlled diamond surface. *Appl. Phys. Express* **2**(5), 055001 (2009). doi:[10.1143/APEX.2.055001](https://doi.org/10.1143/APEX.2.055001)
152. D. Lee, J.M. Blakely, T.W. Schroeder, J.R. Engstrom, A growth method for creating arrays of atomically flat mesas on silicon. *Appl. Phys. Lett.* **78**(10), 1349–1351 (2001). doi:[10.1063/1.1352656](https://doi.org/10.1063/1.1352656)
153. T. Nishida, N. Kobayashi, Step-free surface grown on GaAs (111) B substrate by selective area metalorganic vapor phase epitaxy. *Appl. Phys. Lett.* **69**(17), 2549–2550 (1996). doi:[10.1063/1.117735](https://doi.org/10.1063/1.117735)
154. T. Nishida, N. Kobayashi, Formation of a 100- μ m-wide stepfree GaAs (111)B surface obtained by finite area metalorganic vapor phase epitaxy. *Jpn. J. Appl. Phys.* **37**(1A/B, Part 2), L13–L14 (1998). doi:[10.1143/JJAP.37.L13](https://doi.org/10.1143/JJAP.37.L13)
155. J.A. Powell, P.G. Neudeck, A.J. Trunek, G.M. Beheim, L.G. Matus, R.W. Hoffman Jr., L.J. Keys, Growth of step-free surfaces on device-size (0001)SiC mesas. *Appl. Phys. Lett.* **77**(10), 1449–1451 (2000). doi:[10.1063/1.1290717](https://doi.org/10.1063/1.1290717)
156. T. Akasaka, Y. Kobayashi, M. Kasu, Step-free GaN hexagons grown by selective-area metalorganic vapor phase epitaxy. *Appl. Phys. Express* **2**(9), 091002 (2009). doi:[10.1143/APEX.2.091002](https://doi.org/10.1143/APEX.2.091002)
157. C.E. Nebel, C.R. Miskys, J.A. Garrido, M. Hermann, O. Ambacher, M. Eickhoff, M. Stutzmann, AlN/diamond np-junctions. *Diam. Relat. Mater.* **12**(10–11), 1873–1876 (2003). doi:[10.1016/S0925-9635\(03\)00313-3](https://doi.org/10.1016/S0925-9635(03)00313-3)
158. C.R. Miskys, J.A. Garrido, C.E. Nebel, M. Hermann, O. Ambacher, M. Eickhoff, M. Stutzmann, AlN/diamond heterojunction diodes. *Appl. Phys. Lett.* **82**(2), 290–292 (2003). doi:[10.1063/1.1532545](https://doi.org/10.1063/1.1532545)
159. Y. Taniyasu, M. Kasu, MOVPE growth of single-crystal hexagonal AlN on cubic diamond. *J. Cryst. Growth* **311**(10), 2828–2830 (2009). doi:[10.1016/j.jcrysgro.2009.01.021](https://doi.org/10.1016/j.jcrysgro.2009.01.021)
160. K. Hiram, Y. Taniyasu, M. Kasu, Heterostructure growth of a single-crystal hexagonal AlN (0001) layer on cubic diamond (111) surface. *J. Appl. Phys.* **108**(1), 013528 (2010). doi:[10.1063/1.3452362](https://doi.org/10.1063/1.3452362)
161. M. Imura, K. Nakajima, M. Liao, Y. Koide, Growth mechanism of c-axis-oriented AlN on (111) diamond substrates by metal-organic vapor phase epitaxy. *J. Cryst. Growth* **312**(8), 1325–1328 (2010). doi:[10.1016/j.jcrysgro.2009.09.020](https://doi.org/10.1016/j.jcrysgro.2009.09.020)
162. K. Hiram, Y. Taniyasu, M. Kasu, Hexagonal AlN(0001) heteroepitaxial growth on cubic diamond (001). *Jpn. J. Appl. Phys.* **49**(4s), 04DH01 (2010). doi:[10.1143/JJAP.49.04DH01](https://doi.org/10.1143/JJAP.49.04DH01)
163. S. Tanaka, R.S. Kern, R.F. Davis, Initial stage of aluminum nitride film growth on 6H-silicon carbide by plasma-assisted, gas-source molecular beam epitaxy. *Appl. Phys. Lett.* **66**(1), 37 (1995). doi:[10.1063/1.114173](https://doi.org/10.1063/1.114173)

164. J.A. Powell, J.B. Petit, J.H. Edgar, I.G. Jenkins, L.G. Matus, J.W. Yang, P. Pirouz, W.J. Choyke, L. Cleman, M. Yoganathan, Controlled growth of 3C-SiC and 6H-SiC films on low-tilt-angle vicinal (0001) 6H-SiC wafers. *Appl. Phys. Lett.* **59**(3), 333–335 (1991). doi:[10.1063/1.105587](https://doi.org/10.1063/1.105587)
165. T. Ouisse, Electron transport at the SiC/SiO₂ interface. *Phys. Status Solidi A* **162**(1), 339–368 (1997). doi:[10.1002/1521-396X\(199707\)162:1<339::AID-PSSA339>3.0.CO;2-G](https://doi.org/10.1002/1521-396X(199707)162:1<339::AID-PSSA339>3.0.CO;2-G)
166. N.D. Bassim, M.E. Twigg, C.R. Eddy Jr., J.C. Culbertson, M.A. Mastro, R.L. Henry, R.T. Holm, P.G. Neudeck, A.J. Trunek, J.A. Powell, Lowered dislocation densities in uniform GaN layers grown on step-free (0001) 4H-SiC mesa surfaces. *Appl. Phys. Lett.* **86**(2), 021902 (2005). doi:[10.1063/1.1849834](https://doi.org/10.1063/1.1849834)
167. J.D. Caldwell, M.A. Mastro, K.D. Hobart, O.J. Glembocki, C.R. Eddy Jr., N.D. Bassim, R.T. Holm, R.L. Henry, M.E. Twigg, F. Kub, P.G. Neudeck, A.J. Trunek, J.A. Powell, Improved ultraviolet emission from reduced defect gallium nitride homojunctions grown on step-free 4H-SiC mesas. *Appl. Phys. Lett.* **88**(26), 263509 (2006). doi:[10.1063/1.2218045](https://doi.org/10.1063/1.2218045)

Novel Aspects of Diamond
From Growth to Applications

Yang, N. (Ed.)

2015, XVI, 325 p. 153 illus., 33 illus. in color., Hardcover

ISBN: 978-3-319-09833-3